Energy Conversion and Management 350 (2026) 120968

Contents lists available at ScienceDirect

Energy Conversion and Management

journal homepage: www.elsevier.com/locate/enconman

Development and application of a reduced chemical kinetic mechanism for e-gasoline surrogate fuel in engine combustion modelling

Lorenzo Ferrari [a,*], Massimo Duchi [a], Giuseppe Sammito [b], Marcus Fischer [c], Nicolò Cavina [a]

[a] Department of Industrial Engineering, University of Bologna, Viale del Risorgimento 2, 40136 Bologna, Italy
[b] FEV Italia S.r.l., Via Livorno, 60, 10144 Turin, Italy
[c] FEV Europe GmbH, Neuenhofstraße 181, 52078 Aachen, Germany

ARTICLE INFO

Keywords:
Electrofuels
Chemical mechanism reduction
Distillation curve modelling
Methanol to Gasoline
Combustion modelling

ABSTRACT

Renewable synthetic fuels offer the potential to reduce global carbon dioxide emissions when used in internal combustion engines of current and future passenger car fleets. To enable the simulation of combustion and evaporation behaviour of renewable gasoline fuels, a surrogate fuel algorithm has been developed. This algorithm embeds a physical model of the fuel distillation process and accounts for key properties such as density, research and motor octane numbers, carbon-to-hydrogen ratio, and volumetric oxygen content. The surrogate palette includes isooctane, isopentane, n-heptane, toluene, pseudocumene, and 1-hexene. The fuels studied are standard RON95E10 and its synthetic counterpart, MtG-E10. A reduced chemical reaction mechanism, consisting of 548 species and 3350 reactions, is derived from the Lawrence Livermore National Laboratory mechanism using the Direct Relation Graph with Error Propagation and Sensitivity Analysis reduction method. Laminar flame speed neural networks are generated from this reduced mechanism to support the calibration of the Eddy Burn-Up combustion model within a one-dimensional computational fluid dynamics simulation framework representing a single-cylinder spark-ignited research engine. The model is calibrated and validated for the standard gasoline fuel, then applied to the synthetic fuel as well. Results show that the model accurately predicts combustion behaviour for new gasoline-like fuels without requiring recalibration of the combustion model turbulent flame speed parameters; only the laminar flame speed metamodel needs to be updated when switching fuels. For MtG–E10, the root mean square error remained below 4 bar for peak in-cylinder pressure and within 1 crank-angle degree for the 50 % mass-fraction-burned angle.

1. Introduction

Due to increasing global pressure to tackle climate change and reduce emissions, countries, regions, and cities are continuously announcing drastic emissions cuts. In September 2019, during the United Nations Secretary-General's Climate Action Summit, more than 65 countries and the European Union committed to achieving carbon neutrality by 2050 [1]. To cope with the rise of Greenhouse Gas (GHG) emissions, the European Union (EU) has adopted one of the most ambitious climate policies, synthesised in the legislative package termed the European Green Deal (EGD). This framework aims to achieve net-zero emissions by 2050, aligning with the Intergovernmental Panel on Climate Change (IPCC) scenario that limits global temperature increase to 1.5 °C with respect to preindustrial levels [2]. From this perspective, a mid-term milestone is represented by the Fit for 55 goal, which aims to reduce GHG emissions by 55 %, relative to 1990 levels, by 2030 [3].

The global transport sector is responsible for about 20 % of the total carbon dioxide (CO_2) emissions and relied on fossil fuels for 95 % in 2022, with only a 5 % share on biofuels [4]. In the last decade, these regulations have accelerated the transition towards Electric Vehicles (EVs), referring to them as zero-emission vehicles. However, the zero emissions are only from the tailpipe of the vehicle, while if the overall life cycle is considered, the overall emissions are not null [5]. Moreover, at the moment, low-carbon electricity generation is not prevailing, since electricity around the world is mostly produced from fossil fuels (such as coal, oil, etc.), making the decarbonization of the automotive sector via EVs not effective in reducing GHG emissions [6].

The use of non-fossil-based fuels represents an alternative solution to reduce the carbon footprint in the transport sector. Flexible pathways

* Corresponding author.
E-mail address: lorenzo.ferrari28@unibo.it (L. Ferrari).

https://doi.org/10.1016/j.enconman.2025.120968
Received 28 August 2025; Received in revised form 10 December 2025; Accepted 16 December 2025
Available online 22 December 2025

Nomenclature

0D/1D/3D CFD	Zero-One-Three Dimensional Computational Fluid Dynamics
AFR_{ST}	Stoichiometric Air-To-Fuel Ratio
CHR	Carbon-To-Hydrogen Ratio
CO_2	Carbon Dioxide
COV	Coefficient of Variation
DC	Distillation Curve
DRG	Direct Relation Graph
DRGEP	Direct Relation Graph with Error Propagation
DRGEPSA	Direct Relation Graph with Error Propagation and Sensitivity Analysis
EGD	European Green Deal
EGR	Exhaust Gas Recirculation
ETRF	Ethanol Toluene Reference Fuel
EU	European Union
EV_s	Electric Vehicle
FSN	Filter Smoke Number
GDI	Gasoline Direct Injection
GHG_s	Greenhouse Gases
HC	Unburnt Hydrocarbons
ICE	Internal Combustion Engine
ID	Ignition Delay
IMEP	Indicated Mean Effective Pressure
IPCC	Intergovernmental Panel On Climate Change
IVC	Intake Valve Closing
LFS	Laminar Flame Speed
LHV	Lower Heating Value
MON	Motor Octane Number
MtG	Methanol To Gasoline
NTC	Negative Temperature Coefficient
OP	Operating Point
PN	Particulate Number
PRF	Primary Reference Fuel
PtX	Power to X
RMSE	Root Mean Square Error
RON	Research Octane Number
SA	Spark Advance
SCRE	Single-Cylinder Research Engine
SRK	Soave-Redlich-Kwong
T10/T50/T90	Temperatures at 10 %, 50 %, 90 % evaporated fuel
TDC	Top Dead Centre
TKE	Turbulent Kinetic Energy
TPA	Three Pressure Analysis
TRF	Toluene Reference Fuel
VLE	Vapor-Liquid Equilibrium
VO	Volumetric Oxygen Concentration
VVT	Variable Valve Timing

and advancements in production processes have resulted in the exploitation of biomass for the production of biofuels, which represent a viable substitute for fossil-based fuels [7]. However, sustainable biomass potentials and future costs are subject to fluctuations, and other fuel pathways could be necessary to get to a fossil fuel-independent transport sector [8]. Moreover, the future contribution of biofuels seems insufficient to cope with the expected global transport demand. For instance, Grahn et al. [9] analysed cost-effective fuel choices in the transportation sector under different international climate regimes, proving that biofuels, in the regional caps scenario, actually increase the CO_2 concentration target (at least up to 550 ppm) with biofuels never playing a dominant role in the transportation sector. In this regard, electrofuels (e-fuels) are an attractive solution to fossil-based fuels and biofuels. They are carbon-based fuels produced from CO_2 and water, with electricity as the primary source of energy. Since CO_2 is consumed during their production, their combustion process can be considered carbon–neutral, as the overall carbon dioxide balance is zero [10]. Dieterich et al. [11] proposed a recent literature review about the Power-to-Liquid (PtL) process for methanol, DME and Fischer-Tropsch fuels. PtL integrates renewable power, water electrolysis, carbon capture, fuel synthesis, and product upgrading, closing the carbon cycle and serving as energy storage and carbon capture and utilisation technology. Moreover, Dell'Aversano et al. [12] investigated the production of carbon–neutral synthetic fuels, focusing on e-hydrogen (e-H_2) generated from water electrolysis using renewable electricity and carbon dioxide (CO_2) captured from industrial sites or the air, evaluating these technologies' technological maturity and sustainability, comparing energy conversion efficiency and greenhouse gas emissions with their electric counterparts. As a result of their review, the potential for e-fuels appears to be greatest in the maritime and aviation sectors, while battery electric vehicles are becoming the dominant type in road transport. However, markets for e-fuels in road transport will persist in the upcoming years, as replacing ICE vehicles with electric ones is a gradual process.

Furthermore, e-fuels can benefit from an already existing infrastructure, making transportation and delivery easier and cheaper [13]. Additionally, the drop-in capabilities of e-fuels, namely the fact that they can be employed in current ICEs without requiring any modification, make them a complementary solution to EVs, which could enhance a rapid reduction in GHG emissions [12].

Some studies can be found in the literature addressing the potential of synthetic fuels. For instance, Wouters et al. [14] experimentally investigated 5 different synthetic gasoline fuels, which can be synthesised via the Methanol-to-Gasoline (MtG) process [15], and a reference fossil gasoline. The final MtG gasoline consists of paraffins, olefins, naphthenes and aromatics, mainly in the gasoline boiling range. Isoparaffins are the most abundant component within the synthetic product, which can be used as a drop-in fuel when blended with an octane booster such as ethanol. Kraus et al. [16] investigated several synthetic fuel blends in a single-cylinder spark ignition engine. Among them, methylformate, when blended with alkylate gasoline, showed low particulate number (PN) emissions comparable to pure oxygenated fuels, due to its low boiling point, which favours mixture homogenization. Other studies involved the analysis of POSYN [17], whose composition is nearly free of aromatics, making it an attractive solution to reduce soot emissions. For instance, Albrecht et al. [18] experimentally investigated the emissions production of 4 different fuel compositions, among which the synthetic renewable fuel POSYN showed the lowest particulate matter emissions, thanks to the absence of aromatics in its chemical composition. Rossi et al. [19] also simulated the combustion of such fuel in a 3D CFD environment, via chemical kinetics simulation employing an appropriate surrogate fuel formulation. The laminar flame speeds (LFS) were compared against a premium gasoline fuel, SP98, and POSYN exhibited a higher flame speed value, enhancing the combustion efficiency and reducing knock occurrence.

In this regard, fuel surrogates are hydrocarbon mixtures designed to replicate key properties of a target fuel. They play a crucial role in fuel modelling, as real fuels – such as gasoline and diesel – are complex blends composed of many hydrocarbons [20]. Consequently, representing their combustion behaviour in computational environments is challenging due to both chemical and computational constraints. Moreover, when the combustion of a fuel containing a large number of species is to be modelled, issues arise both because (i) well-established kinetic mechanisms are available only for a restricted number of compounds, and (ii) because accounting for numerous reactions leads to an

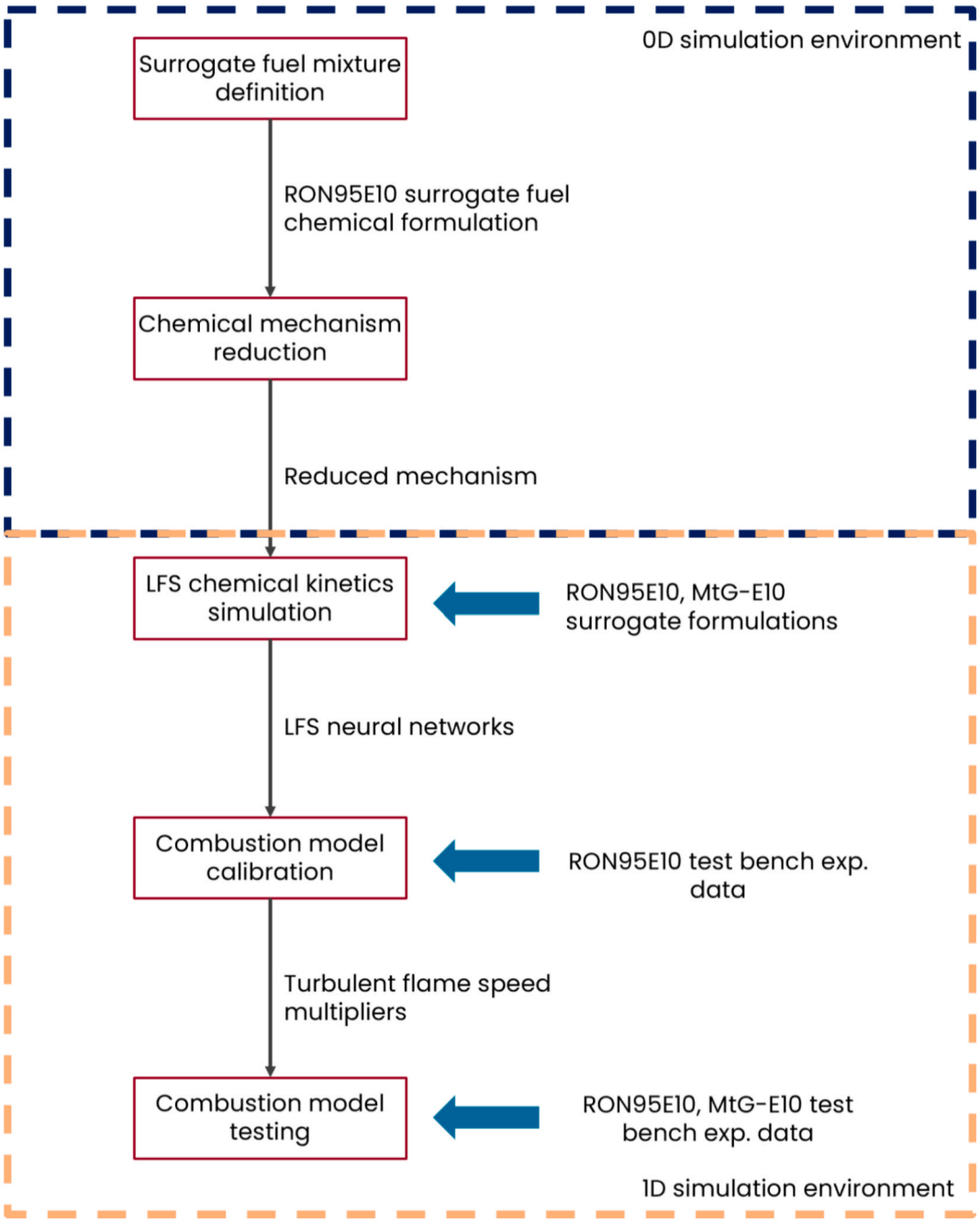

Fig. 1. Overall activity workflow.

impractical computational burden [21]. Thus, reduced mechanisms are typically generated, in which the number of chemical species and reactions is reduced from the original detailed mechanism. Several strategies, such as principal component analysis [22], sensitivity analysis [23], Jacobian analysis [24], detailed reduction [25], path flux analysis [26] and multi-element flux analysis [27] can be employed to perform the mechanism reduction. The direct relation graph (DRG) method was extensively used for mechanism reduction, and it was originally proposed by Lu et al. [28]. The same authors applied DRG methods to get to a skeletal mechanism for n-heptane and isooctane [29]. Moreover, a reduced mechanism for the high-temperature oxidation of biodiesel surrogates was developed by Luo et al. [30] employing DRG methodology. The DRG reduction method was further improved by Pepiot-Desjardins et al. [31], who extended the DRG to DRG with error propagation (DRGEP). DRG was coupled with sensitivity analysis by Zheng et al. [32], ending up with the DRGSA method. In this regard, sensitivity coefficients are calculated for all the species not removed by DRG for several temperatures, pressures and equivalence ratios. The sensitivity coefficient is defined as the worst-case relative error induced, for instance, in the ignition delay due to the elimination of a certain species. As a consequence, removing species with a sensitivity coefficient lower than a user-defined threshold has a limited effect on the ignition delay accuracy, and the mechanism can be further reduced from the DRG. Eventually, Niemeyer et al. [33] merged the DRGSA and the DRGEP methods into the DRGEPSA, a direct relation graph with error propagation and sensitivity analysis. Basically, at first, DRGEP is performed to efficiently remove unimportant species, and the sensitivity analysis is then carried out to further reduce the chemical reaction mechanism for a given error limit.

When it comes to defining proper surrogate fuels, several approaches

can be found in literature, dealing with Primary Reference Fuels (PRF), to match fuel Research Octane Number (RON), Toluene Reference Fuels (TRF), to also account for Motor Octane Number (MON), or more complex mixtures [34]. However, multi-component mixtures are required as surrogate fuels if additional properties like the distillation curve, functional group or hydrocarbon class distribution, average molecular weight and octane sensitivity have to be reproduced [34]. To enable chemical kinetic simulations without a heavy computational burden, a comprehensive chemical reaction mechanism, including all the chemical species found in the multi-component surrogate, has to be reduced. For example, Chen et al. [35] developed 2 reduced mechanisms for a 5-component gasoline surrogate, including toluene, isopentane, isooctane, n-pentane and n-heptane with 107 and 207 species, respectively, from the extended version of the Lawrence Livermore National Laboratory (LLNL) mechanism [36]. Andrae et al. [37] and Zhong et al. [38] conceived reduced mechanisms for gasoline surrogates with 143 and 89 species, respectively, including the oxidation pathways of isooctane, n-heptane, ethanol, toluene and di-isobutylene. Cycloalkanes were not included in these mechanisms, even though they can account for up to 16 % volume concentration in some gasoline fuels [39].

In this work, a reduced mechanism for e-gasoline surrogates is developed starting from the detailed mechanism of the Lawrence Livermore National Laboratory [40]. First, the DRGEPSA method is applied to decrease the complexity of the mechanism, which includes the chemistry of 7 single-component fuels representing the major species typically found in gasoline fuels, namely isooctane, n-heptane, toluene, pseudocumene, isopentane, 1-hexene and ethanol. Moreover, a surrogate fuel algorithm is conceived to reproduce multiple fuel properties like density, RON, MON, Carbon-to-Hydrogen Ratio (CHR), Oxygenate Volume fraction (VO), and the fuel distillation curve (DC) profile. The developed algorithm is then applied to standard fossil RON95E10 gasoline fuel and to a synthetic gasoline, that is MtG – E10. The Eddy-Burn Up combustion model, embedded into the GT-Suite one-dimensional computational fluid dynamics (1D-CFD) simulation environment, is calibrated against experimental data regarding RON95E10 fuel, and subsequently applied to MtG – E10 to assess its predictive capability while switching fuel kinds. This methodology aims to overcome a limit of the 1D CFD simulation environment (GT-Suite [41]), which is related to the possibility of simulating the combustion of different gasoline-like fuel compositions. As a matter of fact, the software allows for the simulation of just one standard gasoline fuel; thus, the original contribution of this work is addressing and validating a methodology to achieve fuel flexibility combustion simulations.

The study is organised as follows: Section 2 highlights the overall methods, which describe the theoretical background of the surrogate fuel algorithm and the chemical reaction mechanism reduction. In Section 3, the results are presented and discussed, and in Section 4, the main conclusions are drawn.

2. Methods

Starting from an existing 1D CFD model, representative of the single-cylinder research engine employed in this study, the results from the surrogate fuel algorithm were utilised to model the combustion of the fuels under analysis. In this study, a physical model regarding the fuel distillation curve was developed and validated against available experimental distillation curve profiles from the literature. By doing so, the resulting surrogate fuel is also representative of the real fuel evaporation behaviour. As the next step, the RON95E10 surrogate fuel formulation was employed to reduce the comprehensive chemical reaction mechanism [40], in which ignition delay simulations were utilised to eliminate unnecessary chemical species and reactions by the DRGEPSA algorithm. Then, the reduced mechanism was used for chemical kinetics LFS simulations, whose results were subsequently integrated into the Eddy-Burn Up combustion model [42,43] through a neural network approach.

Once the neural network was defined, the RON95E10 surrogate formulation was integrated into the GT-Suite simulation environment as a fluid mixture, and to come up with reference burn rate profiles to calibrate the combustion model, the Three-Pressure-Analysis (TPA) was carried out. This kind of simulation takes experimental boundary data like the in-cylinder pressure, the intake and exhaust port pressures, the valve lifts/timings, the valve tumble coefficients, the spark timing, the boundary intake and exhaust temperatures and the intake EGR fraction to estimate the in-cylinder conditions at intake valve closing (IVC). Other outputs of the TPA are the fuel burn rate and the simulated in-cylinder pressure when the estimated burn rate is imposed in the model. The calibration of the Eddy-Burn Up combustion model was performed in closed volume conditions, starting from the TPA IVC results, where the reference burn rate profiles were compared to the predicted ones by the combustion model. The latter was optimised in its turbulent flame speed parameters, using 18 of the 23 engine operating points available for RON95E10 fuel, and validated against the remaining 5.

The calibrated combustion model was, eventually, tested using the RON95E10 synthetic fuel counterpart, that is MtG – E10, with the same methodology without recalibrating it. Fig. 1 highlights the workflow followed to carry out the analysis.

Table 1
HELEN engine hardware specifications.

Engine type	Single-cylinder, 4-stroke
Piston	Flat
Combustion chamber	Hemispherical
Displaced volume	500 cc
Stroke × Bore	113.2 × 75 mm
Stroke/Bore ratio	1.51
Connecting rod length	220 mm
Crank radius	56.6 mm
Compression ratio	10.8
Number of valves	4
Injection type	Direct
Valve timing	Variable
Max. peak cylinder pressure	180 bar
Max. fuel pressure	200 bar
Fuel injector	6-hole solenoid

2.1. Experimental setup

The experimental data for this study were provided by FEV Group GmbH. A single-cylinder research engine (SCRE) was utilised for data acquisition, and the main engine characteristics are reported in Table 1. For fuel injection, a centrally mounted six-hole solenoid-actuated series production injector was employed, together with an intake stroke injection strategy to attain homogeneous operation. Moreover, the cylinder was equipped with a centrally mounted spark plug, and two piezoelectric transducers for the in-cylinder pressure measurement were oppositely mounted between the intake and exhaust valves. The intake and exhaust manifolds were fitted with pressure transducers as well. A hot-film air mass meter was used to measure the intake air mass flow, while a Coriolis-type mass flow sensor measured the fuel mass flow. To keep the imposed engine speed and load, the engine was coupled with an electric dynamometer and an eddy-current brake, respectively. To maintain the desired delta pressure between intake and exhaust, an external boosting system and an exhaust gas backpressure control valve were employed. For the exhaust gas components measurement (HC, CO, CO_2, NO_X, O_2), a partial exhaust gas mass flow was utilised to sample the species upstream of the backpressure control valve. Soot emissions were quantified by the filter smoke number (FSN) and measured downstream of the backpressure control valve. Eventually, HC emissions were measured as C_3H_8. 200 cycles were recorded for each engine operating point (OP), and the mean quantities were used as input data for the present analysis. The coefficient of variation (COV) for the indicated mean effective pressure (IMEP) was calculated, and all the engine

Table 2
Fuels properties.

Property	RON95E10	MtG – E10
Density @ 15 °C [kg/m^3]	746.40	744.10
Lower heating value [MJ/kg]	41.59	41.40
Molar mass [g/mol]	87.70	88.20
RON/MON [-]	96.7/85.5	96.6/85.9
T10 [°C]	49.50	47.50
T50 [°C]	86.40	67.80
T90 [°C]	154.30	151.30
Vapor pressure DVPE [kPa]	58.80	71.50
C/H/O mass share [-]	6.05/11.93/0.19	6.08/11.83/0.2
Air-to-fuel ratio [-]	14.08	14.02
Aromatics [% V/V]	26.30	30.60
Olefines [% V/V]	9.40	4.14
Saturated hydrocarbons [% V/V]	54.70	55.26
Alcohols [% V/V]	9.50	10.00

Table 3
Investigated engine OP$_s$ for MtG – E10.

Engine speed [1/min]	IMEP [bar]	EGR [%]
2500	16	0–25
2500	3–21	0

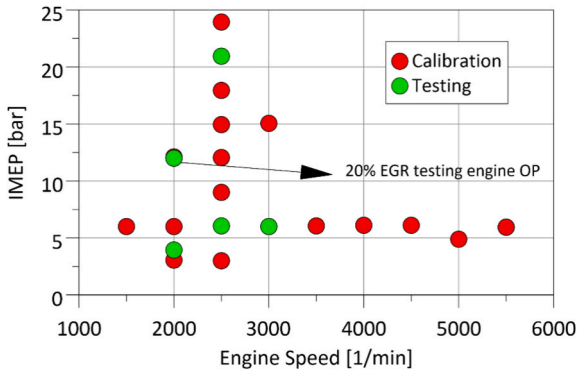

Fig. 2. RON95E10 fuel engine OP$_s$ under analysis.

operating points showed a value lower than the threshold limit of 5 %, meaning that the mean engine cycle is representative of the specific engine conditions. Additional details about the specifications of the test cell measurement instruments can be found in the Appendix.

As mentioned in the Introduction section, 2 fuels were tested, and their characteristics are reported in Table 2. As can be seen, MtG – E10 can be regarded as the synthetic counterpart of the standard RON95E10 since the properties are similar. Anyway, some differences can be spotted regarding the T50 temperature, that is, the temperature at which half of the fuel volume is recovered from the distillation process.

As for the experimental data collection, the tested engine OP for MtG – E10 are reported in Table 3. Instead, for the RON95E10, a wider range of the engine map was investigated. 23 engine operating points, ranging from several engine speeds, loads and EGR%, were considered for the predictive combustion model calibration and testing. In particular, 18 of them were used to calibrate the combustion model, while the remaining 5 were employed for model testing (Fig. 2). The experimental data are coming from a wider investigation carried out by Wouters et al. [14], where several synthetic fuels were tested, and for confidentiality reasons, the collected data regarding the in-cylinder pressure traces cannot be shared. The present author decided to focus, in this investigation, on both standard RON95E10 and its synthetic counterpart, that is, MtG-E10.

2.2. Single-cylinder engine model

The simulations were carried out using the commercial 1D simulation tool, GT-POWER version 2023, provided by Gamma Technologies [41]. The base model setup resembles the Three-Pressure-Analysis one. Boundary pressure templates are meant to impose the measured intake and exhaust manifold dynamic pressure, as well as the average intake and exhaust manifold temperature. Material properties of the runners were included in the respective templates, and the thermal properties were populated with the density, specific heat and thermal conductivity of the wall pipe elements. The convective heat transfer is presumed to be defined by the Colburn analogy, which takes into account the fluid velocity, the thermo-physical properties and the wall surface roughness. Intake and exhaust valve discharge coefficients were experimentally characterised and integrated into the model.

As for the in-cylinder heat transfer model, the Cylinder Wall Temperature Solver (EngCylTWallSoln) and the Finite Element Cylinder Structure Geometry (FECylinderStructure) were employed to better predict the heat transfer between the cylinder, the piston, the head and the walls. Heat transfer coefficients between the in-cylinder elements were kept to their default value, while the coolant and oil boundary condition temperatures were taken from the test bench data. Moreover, owing to the importance of the heat transfer and the turbulent flow interaction on the combustion prediction, the flow in-cylinder heat transfer model was chosen instead of the Woschni one. The flow heat transfer model is based on the effect of swirl, tumble and turbulence on the heat transfer prediction. The flow details provided by the K–k–ε turbulent flow model were employed to compute the convective heat transfer coefficient, h, to the walls by using the Colburn analogy [43]. The 0D turbulence model was already previously calibrated against a reference 3D CFD cold flow simulation carried out at 2000 1/min and 15 bar of indicated mean effective pressure (IMEP). The results of this calibration activity are being reported on another work of the present authors, currently still under review.

2.3. Surrogate fuel algorithm – Fuel properties

An appropriate surrogate fuel mixture is essential to reproduce key properties of the fuel under investigation. In this context, it is paramount to represent the fuel characteristics that are most relevant to combustion using a surrogate blend composed of a limited number of species. These key attributes, which the surrogate must replicate, are commonly referred to as target properties.

Target properties are broadly distinguished into chemical and physical classes. In the context of three-dimensional computational fluid dynamics (3D CFD) modelling, particularly for Gasoline Direct Injection (GDI) systems, physical properties such as density, viscosity, and volatility are of primary importance. These attributes critically influence the modelling of in-cylinder flow dynamics, spray atomization, and fuel–air mixture formation [44,45].

In contrast, chemical properties retain their significance even in modelling frameworks where spatial resolution is minimal or absent, such as in lumped parameter approaches. This is due to the fact that the oxidation behaviour of the air–fuel mixture is intrinsically governed by the molecular structure of the fuel [34]. For instance, in zero-dimensional models that approximate turbulent combustion in spark-ignition (SI) engines, the laminar flame speed emerges as a pivotal parameter [46]. This parameter can be rigorously computed via chemical kinetics simulations, which rely on chemical reaction mechanisms that encompass the formation and consumption of intermediate species, as well as the associated heat release processes [34].

Among the chemical features commonly employed for fuel characterisation, the RON and MON are typically targeted. Another fundamental chemical parameter is the Carbon-to-Hydrogen Ratio (CHR), which quantifies the relative abundance of carbon and hydrogen atoms in a given fuel. The CHR is directly indicative of the fuel's molecular

Table 4
Target properties and selected chemical species for the surrogate palette.

Chemical species	Target properties
N-heptane	Liquid density
Iso-octane	CHR
Iso-pentane	RON
Toluene	MON
Pseudocumene	VO
1-hexene	Distillation curve
Ethanol	

structure and bears a strong correlation with several critical properties, including density, lower heating value (LHV), and combustion characteristics such as flame propagation speed and adiabatic flame temperature [21].

In addition, the concentration of oxygenated compounds in a fuel significantly influences its performance. Ethanol, for example, is commonly blended with gasoline-like fuels to enhance engine efficiency and reduce emissions. Moreover, as mentioned in the Introduction section, the evaporation behaviour of the target fuel is another key feature to be reproduced if the goal is to get to a more representative surrogate fuel formulation. To sum up, the addressed target properties are density, CHR, RON/MON, VO and the fuel distillation profile (Table 4).

2.4. Surrogate fuel algorithm – Target chemical species

Fuel combustion behaviour is strongly affected by its chemical composition, which in turn influences key combustion-related parameters such as volatility, ignition delay, vaporisation, and heat release [44]. The hydrocarbons found in gasoline-like fuels are typically categorised into five main classes: n-paraffins, *iso*-paraffins, olefins, naphthenes, and aromatics. When a fuel's composition is described according to these hydrocarbon classes, it is referred to as its PIONA composition. Fig. 3 illustrates molecular structures that are representative of each PIONA category.

To effectively replicate the behaviour of gasoline-like fuels, it is essential that the selected surrogate components encompass a molecular size range between C5 and C10, which corresponds to the majority of constituents typically found in such fuels. This consideration is particularly critical for accurately reproducing the fuel's distillation curve (DC), as the boiling point of hydrocarbons is closely correlated with molecular size. Real spark-ignition (SI) engine fuels exhibit a wide distillation temperature range, generally extending from approximately 25 °C to 170 °C [45]. By analysing the literature, several studies can be found related to the formulation of surrogate fuels. In these studies [21,44,47,48], isooctane, n-heptane, and toluene emerge as reference chemical species to model the laminar flame speeds and ignition delays of gasoline fuels by constituting the TRF surrogate fuel. However, when properties like the fuel distillation curve, the functional group or hydrocarbon class distribution, and average molecular weight need to be reproduced, more chemical species have to be included in the palette. In this work, the target fuel properties to be replicated by the surrogate fuel, made up of a proper combination of selected hydrocarbon species, are reported in Table 4. Among the usual TRF chemical species, the *iso*-pentane and pseudocumene are included in the surrogate palette to reproduce the initial and final distillation curve, as the boiling temperatures are respectively 28.1 °C and 168 °C. Moreover, 1-hexene was selected as the representative chemical species for the olefin hydrocarbon class, while ethanol was selected for the oxygenates. Cycloalkanes were not included in the surrogate palette like in other studies of Andrae et al. [37], Zhong et al. [38], who developed skeletal mechanism for gasoline surrogate fuels, in which such hydrocarbon class was not considered, even though they can account for up to 16 % in real gasolines [34].

2.5. Surrogate fuel algorithm – Target properties modelling

The algorithm implemented to generate the two multi-component fuel surrogates is based on the minimisation of a cost function, which accounts for the deviation of the surrogate mixture's properties from their real counterparts. To enable cost function formulation, mixture properties – which need to be compared with real fuel ones – must be estimated.

Surrogate liquid density at 20 °C, ρ_s, can be modelled as [44]:

$$\rho_s = \sum_{i=1}^{N} v_i \rho_i \tag{1}$$

ρ_i, $i = 1, \ldots, N$ are pure components' liquid densities at 20 °C, N is the number of species included in the palette and v_i is the volume fraction of the i-th pure component in the surrogate blend.

Analogously, the surrogate CHR, CHR_s, can be estimated as the ratio between the molar-fraction-based average carbon atoms number and the molar-fraction-based average hydrogen atoms number, namely [44]:

$$CHR_s = \frac{\sum_{i=1}^{N} x_i n_{C,i}}{\sum_{i=1}^{N} x_i n_{H,i}} \tag{2}$$

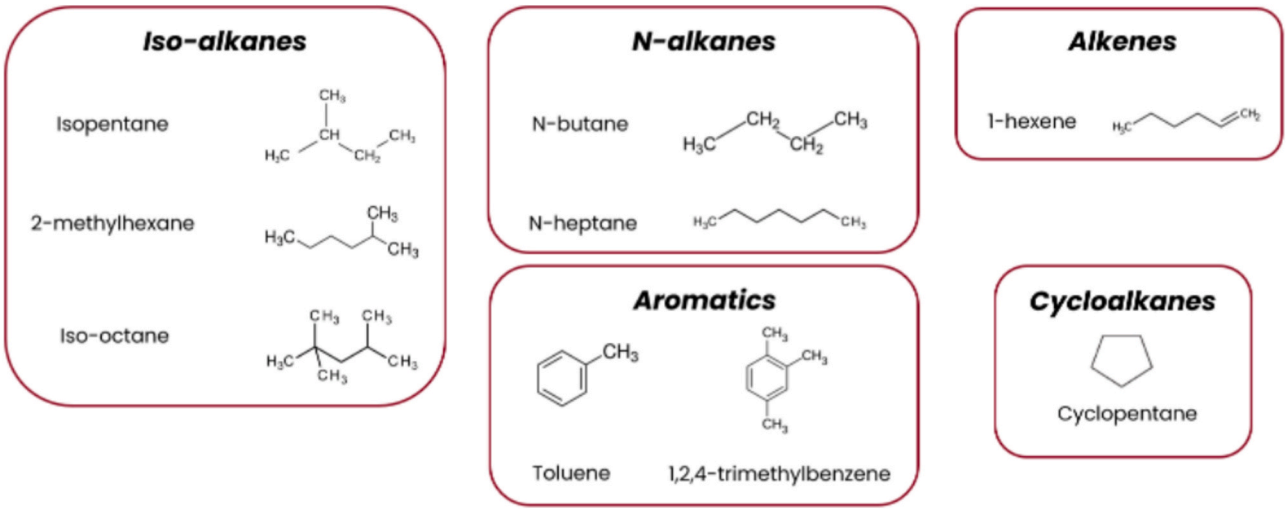

Fig. 3. Molecular structures of gasoline components representative of the PIONA classes (adapted from 47).

where $n_{C,i}$ and $n_{H,i}$ are the number of carbon and hydrogen atoms contained in the molecular structure of the i-th pure component, respectively, while x_i is the molar fraction of the i-th species in the mixture.

Conversely, when it comes to modelling the surrogate RON and MON, a linear mixing rule is likely to produce inaccurate results – as pointed out in [45,49] – especially if an oxygenated hydrocarbon, such as ethanol, is included in the hydrocarbon mixture. Consequently, the following mixing rule, accounting for the non-linearity of RON and MON w.r.t. alcohol molar fraction, has been adopted to model surrogate octane ratings [49]:

$$RON_s = \sum_{i=1}^{N} x_i RON_i + k_{RON} x_a (1 - x_a) \left(RON_a - \sum_{i=1, i \neq a}^{N} x_i RON_i \right) \quad (3)$$

$$MON_s = \sum_{i=1}^{N} x_i MON_i + k_{MON} x_a (1 - x_a) \left(MON_a - \sum_{i=1, i \neq a}^{N} x_i MON_i \right) \quad (4)$$

Here RON_s and MON_s are RON and MON estimations for the surrogate, respectively, while RON_i and MON_i are RON and MON of the i-th pure component, respectively. Additionally, in Eqs. (3) and (4), a is the index associated with the oxygenate present within the palette – i.e., $i \equiv a$ when the i-th pure component considered is ethanol, in this case – while $k_{RON} = 0.45$ and $k_{MON} = 0.94$ are two tuning coefficients, whose values have been defined according to [49,50]. With this blending rule, the reported deviations claimed by the authors [49] are within 0.8 for RON and 0.5 for MON when ethanol is used as a gasoline octane booster.

Since the optimisation process depends on volume fraction composition as the optimisation variable, the calculation of the VO present within the surrogate can be directly performed by the summation of the volume fractions associated with oxygenates present within the palette.

Finally, to estimate the distillation profile of the surrogate, a physical model replicating the experimental procedure detailed in the EN 3405 standard [51] has been implemented. This model, following the approach proposed in [50], is based on Vapour-Liquid Equilibrium (VLE) calculations and employs the Soave-Redlich-Kwong (SRK) equation of state to describe the thermodynamic behaviour of the hydrocarbon mixture in both liquid and gas phases [52]. Additional details about the modelling of the physical distillation process are provided in the Supplementary Material.

2.6. Chemical mechanism reduction

A variety of studies can be found in the literature regarding gasoline surrogate fuels, as pointed out by Sarathy et al. [34], in which comprehensive chemical reaction mechanisms for multicomponent surrogate fuels are reported. Anyway, their usage is impractical from the CFD engine simulation point of view due to the required huge computational time [53]. In this study, the DRGEP chemical mechanism reduction procedure was employed to reduce the comprehensive LLNL mechanism [40], targeting the 7 chemical species used for the surrogate fuel definition. Firstly developed by Pepiot-Desjardins et al. [31], this method considers the path dependence of a target species on others. Following the first pairwise relation defined by Lu et al. [28], Pepiot-Desjardins et al. revised the normalisation by addressing the maximum absolute rate between production and consumption reactions in case that the rate-controlling reaction is dominated by the rapid pseudo-equilibrium reaction [54].

In DRGEP, the error propagation is taken into account by a geometric damping in the selection procedure [31]. When the consumption or production of species A relies on species B, if some error is introduced in the prediction of the latter species, the longer the way this error has to propagate to reach target species A, the lower the effect will be. In this way, a finer selection of the chemical paths is achieved for the accurate prediction of the set of target species. Subsequently, sensitivity analysis was performed to further reduce the mechanism by eliminating the species according to a user-defined error threshold, set in this study to 20 %.

Table 5
Thermodynamic conditions for ignition delay simulations.

Pressure [bar]	Unburnt mixture temperature [K]	Equivalence ratio [–]
5	600	1
5	657	1
5	714	1
5	772	1
60	600	1
60	733	1
60	867	1
60	1000	1
115	678	1
115	785	1
115	893	1
115	1000	1

Table 5 reports the thermodynamic conditions employed to carry out 0D ignition delay simulations for the reduction process. Since all the engine operating points are investigated at stoichiometric operation, the equivalence ratio was always kept at 1, making the final reduced mechanism valid only at stoichiometric conditions, which is the interest of the present authors. Closed volume adiabatic homogeneous reactor simulations, employing the Converge chemistry tool [55], were used to compare the reduced mechanism versus the detailed one. The ignition delay was defined as the time interval between the start of the simulation and the time instant corresponding to a temperature rise of 400 K.

In the next section, the results related to each of the activity steps will be introduced and discussed.

3. Results and discussions

The following sections highlight the results of the method, whose theoretical background is given in Section 2. Specifically, the physical model of the distillation curve will be validated against available literature data, whereas the surrogate fuel algorithm performance will be compared with the real fuel target properties. Moreover, the chemical mechanism reduction results will be introduced and discussed, and finally, the combustion model calibration and testing will be outlined.

3.1. Distillation curve physical model validation

The DC physical model was validated by comparing experimental literature data with the simulation results. The tested fuel compositions are reported in Table 6. Such compositions are given as input to the DC model, and only distilled volume fractions between 5 % and 90 % were considered, as near the initial and final boiling points, experimental inaccuracies may arise. As Fig. 4 shows, the model can accurately reproduce the main distillation features regardless of the mixture complexity. Some deviations could be spotted in the second part of the distillation process, and this could be due to the inaccurate description of the heat transfer between the flask walls and the vapours as the distillation process goes on. Anyway, the 3 key distillation temperatures, namely the T10, the T50 and the T90, are correctly captured by the physical model as the maximum relative error is always below 8 % for all the mixtures considered, with the best performance achieved near the end of the distillation process.

This is paramount since those temperatures represent the fuel's early, mid and late evaporation, the surrogate algorithm should reproduce. Mixture 3 shows almost a flat behaviour since the 2 components, n-decane and pseudocumene (1,2,4-Trimethylbenzene), have similar boiling temperatures. Instead, mixture 4 includes the n-dodecane, which has a higher boiling temperature than pseudocumene of around 50 °C, resulting in a steeper distillation profile. For mixtures 5 and 6, only the head temperatures are available, while for mixture 7, only the kettle temperature was correctly reported in the work of Bruno et al. [56].

Table 6
Fuel compositions used for the distillation physical model validation.

Chemical species	Mix. 1 [56][V/V %]	Mix. 2 [56][V/V %]	Mix. 3 [56][V/V %]	Mix. 4 [56] [V/V %]	Mix. 5 [57][V/V %]	Mix. 6 [57][V/V %]	Mix. 7 [56][V/V %]
Isooctane	0	40	0	0	42	1.1	5
N-heptane	0	0	0	0	12.26	4.16	0
Toluene	20	0	0	0	45.74	40.14	20
Methylcyclohexane	20	0	0	0	0	0	5
N-decane	60	60	80	0	0	0	25
N-dodecane	0	0	0	80	0	0	25
N-tetradecane	0	0	0	0	0	0	20
1,2,4-Trimethylbenzene	0	0	20	20	0	0	0
Isopentane	0	0	0	0	0	55	0

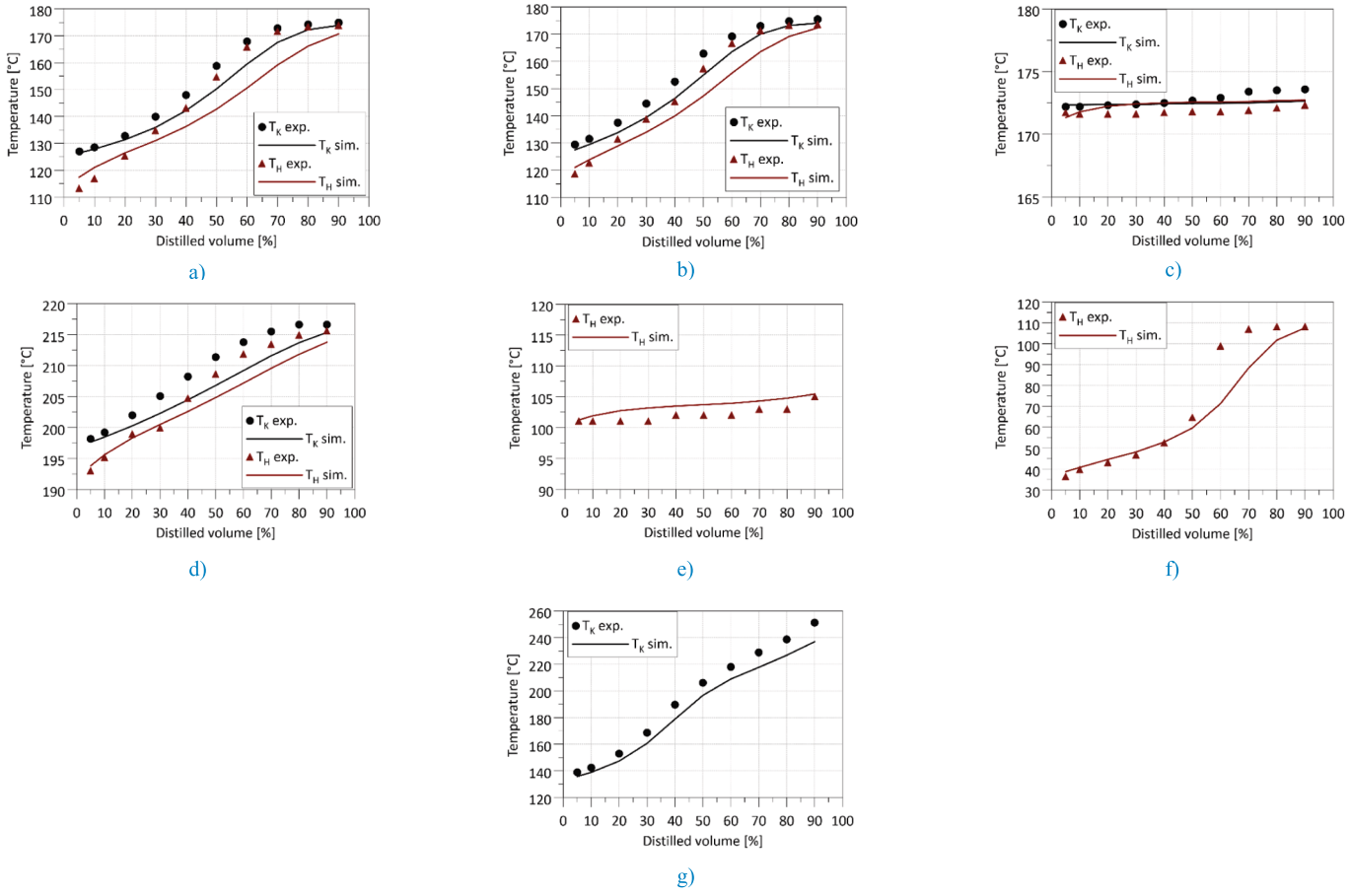

Fig. 4. Distillation model results: (line) physical model, (symbols) experimental values: (a) Mix. 1, (b) Mix. 2, (c) Mix. 3, (d) Mix. 4, (e) Mix. 5, (f) Mix. 6, (g) Mix. 7.

Mixture 6 is affected by a higher error in the T60-T70 range, most likely due to the abrupt vapour composition change from isopentane to toluene, which have very different boiling points.

In the next section, the application of the distillation model to the surrogate generation algorithm will be introduced, together with the main properties of the 2 surrogate fuels.

3.2. Surrogate fuel compositions

By providing the characteristics of the two multi-component fuels (RON95E10 and MtG – E10), addressed in this work, as input target properties to the surrogate generation algorithm, two surrogate fuel formulations were obtained. Their chemical compositions are reported in Table 7, while in Table 8, the surrogate fuel properties are compared to their real counterparts. As for RON95E10 fuel, the initial and mid distillation phases are well captured by the surrogate fuel. A higher deviation can be seen for the T90, which is 11 °C lower than the real fuel. This might lead to reduced predicted soot emissions and particulate matter, as the T90 is well correlated to such pollutants [58],[59]. The octane numbers are affected by a non-negligible deviation, which leads

Table 7
Fuel's surrogate chemical compositions.

Chemical species	RON95E10 [vol. %]	MtG – E10 [vol. %]
Iso-octane	7.310 %	1.302 %
Iso-pentane	27.623 %	34.115 %
N-heptane	10.045 %	5.990 %
Toluene	15.123 %	9.115 %
Pseudocumene	19.810 %	21.615 %
1-hexene	10.435 %	17.969 %
Ethanol	9.654 %	9.896 %

Table 8
Surrogate properties absolute error.

Property	RON95E10 surrogate	RON95E10	Absolute delta	MtG-E10 surrogate	MtG-E10	Absolute delta
Density [kg/m^3]	742.626	741.800	0.826	729.583	739.600	−10.017
CHR [-]	0.536	0.507	0.029	0.523	0.514	0.009
RON [-]	95.011	96.700	−1.689	95.261	96.600	−1.339
MON [-]	86.867	85.500	1.367	86.932	85.900	1.032
VO [-]	0.097	0.095	0.002	0.099	0.100	−0.001
T10 [°C]	50.984	49.500	1.484	45.125	47.500	−2.375
T50 [°C]	81.518	86.400	−4.882	70.294	67.800	2.494
T90 [°C]	143.009	154.300	−11.291	146.280	151.300	−5.020
AFR_{st} [-]	13.855	14.080	−0.225	13.890	14.020	−0.130
LHV [MJ/kg]	41.396	41.590	−0.194	41.515	41.400	0.115

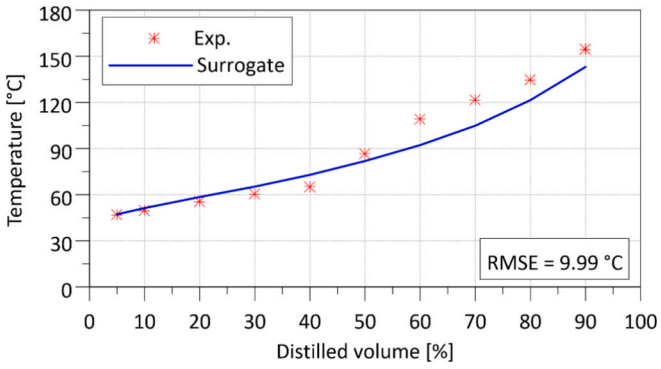

Fig. 5. RON95E10 surrogate fuel distillation curve.

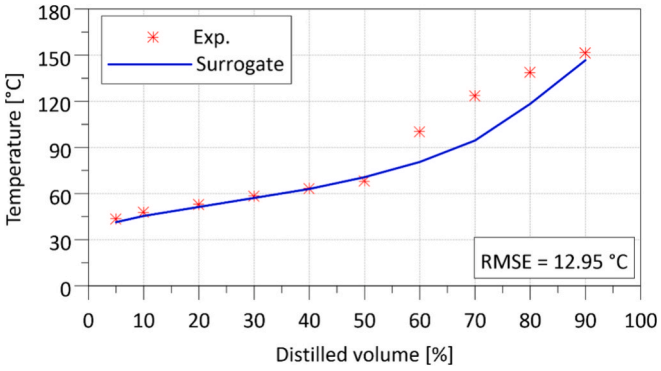

Fig. 6. MtG-E10 surrogate fuel distillation curve.

to a lower surrogate fuel knock resistance, being the RON lower of 1.7 units than the target one. Nevertheless, being the surrogate fuels employed for LFS chemical kinetics simulations, it is crucial that the CHR is well reproduced as highly correlated with the adiabatic flame temperature and flame propagation speed [21]. The algorithm tries to find a compromise between the RON95E10 octane sensitivity, namely the difference between RON and MON, and the tail of the distillation profile by leveraging the amount of pseudocumene. The latter has, at the same time, a high boiling point (168 °C) and a low octane sensitivity (1.5) [60]. Therefore, there must be a trade-off between the octane numbers and the T90 temperature. On the other hand, being the T50 well reproduced by both surrogate fuels, the real fuel evaporation under cold start conditions, particularly affected by the T50 [34], is likely to be properly modelled by such compositions. Figs. 5 and 6 depict the 2 surrogate fuels' distillation profiles compared to the real ones. The RMSE of the full distillation profiles of both fuels is around 10 °C, mainly due to some inaccuracies at the T60-T70, while towards the end of the distillation profiles, the deltas are improved. As for the other properties of the MtG-E10 surrogate, the latter can match with better accuracy all the properties, even though a deviation in the RON of 1.3 is obtained, for the aforementioned reason.

Moreover, the ethanol volumetric concentration is basically imposed by the optimisation algorithm equal to the real fuel one, being the only alcohol available in the palette. Isopentane is mainly used by the optimiser to match the initial boiling temperature and the octane number. The aromatic compounds, instead, keep the surrogate fuel density close to the target one, being the chemical species with the highest density value. In addition, as a remark, both the AFR_{st} and the LHV are not target properties to be reproduced, but they are just derived properties from the resulting surrogate composition.

Once the surrogate fuels were generated, the comprehensive LLNL chemical reaction mechanism [40] was reduced in order to allow the possibility of simulating the surrogate fuels' laminar flame speeds with a reduced computational burden.

3.3. Mechanism reduction

As mentioned in Section 2.6, the detailed mechanism developed by the Lawrence Livermore National Laboratory [40] was reduced by employing the DRGEPSA reduction methodology with the RON95E10 surrogate fuel chemical composition. Prior to the reduction procedure, the detailed mechanism was incorporated with NO_x chemistry from the San Diego combustion institute [61], resulting in an overall mechanism consisting of 1965 species and 10,330 reactions. As a first step, via DRGEP, species and reactions not crucial to describe the oxidation process of the target chemical species, which are all the ones present in the surrogate palette of Table 7, plus N_2, O_2, OH and all the C0 and C1 species, were eliminated. This selection allows targeting the fuel decomposition, oxidation, and H_2-O_2 reactions in the reduced mechanism [26]. The chosen worst-case error for the DRGEP and the SA was 20 %, which resulted in a reduced mechanism of 548 species and 3350 reactions. The achieved mechanisms dimension allows the possibility of performing 1D chemical kinetics simulations, especially regarding the laminar flame speed over a wide range of engine thermodynamic conditions, which would be unbearable from the computational resources point of view with the comprehensive mechanism. The final size of the mechanism is far from being a skeletal version, like the one proposed by Chen et al. [35]. In their work, the resulting mechanism from the DRGEP has a dimension of 720 species, which was further reduced by employing the quasi-steady-state assumption to remove intermediate species. This last reduction procedure was not used by the present authors since the main simulation environment is a 1D CFD one, and for the paper's scope and methods, the final mechanism size was enough to generate a proper grid of LFS in a reasonable amount of time. Moreover, the target species in this study include 2 aromatics, toluene and pseudocumene, which in general have complex oxidation pathways involving many intermediate species [62,63,64], making it complex for the reduction algorithm to both keep accuracy and downsize the mechanism. To compare the size of the present mechanism with others present in literature, Cai et al. [65] developed a reduced mechanism for gasoline ETRF surrogate compositions, finally consisting of 339 species and 2791 reactions, which can be

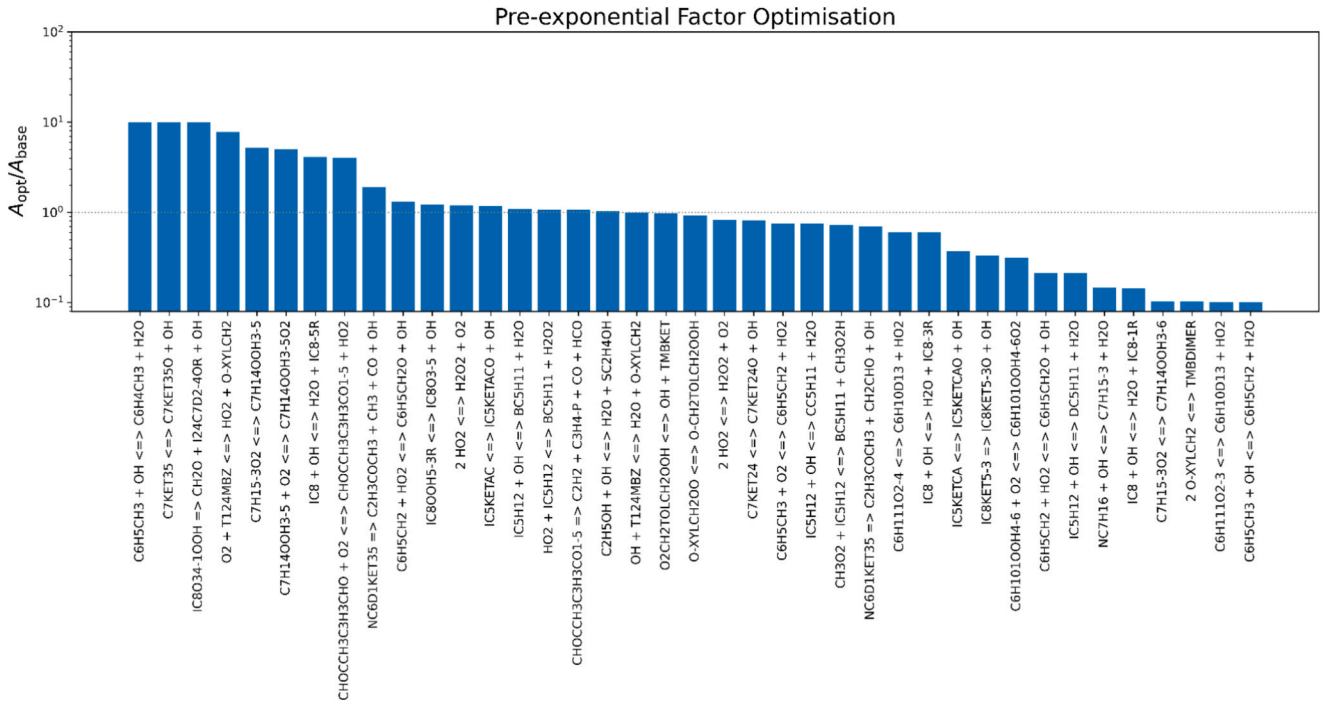

Fig. 7. Pre-exponential factors tuning.

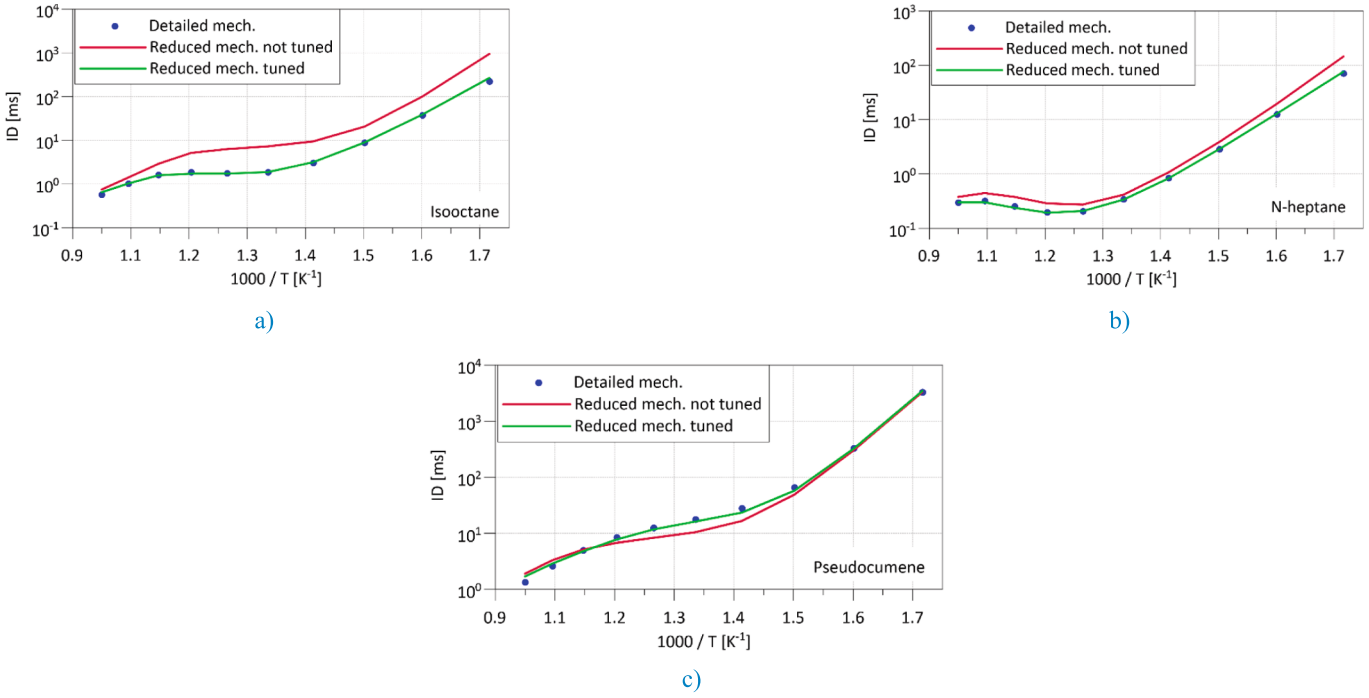

Fig. 8. Chemical reaction mechanism tuning: (a) Isooctane, (b) N-heptane, (c) Pseudocumene.

employed to predict the formation of Polycyclic Aromatic Hydrocarbon (PAH) formation in gasoline engines. Moreover, another similar mechanism size can be found still for ETRF by Mehl et al. [66] featuring 323 species and 2469 reactions, which could be comparable with the one developed in this work, given the higher number of target chemical species. Once DRGEPSA was completed, reaction rates were optimised to reproduce the ignition delay times of the single species found in the surrogate palette coming from the detailed mechanism. This step was performed to compensate for the effect of the reduction of the different chemistry pathways, keeping the global oxidation rate of the fuel as similar as possible to the one predicted by the detailed mechanism. In this regard, for each of the chemical species involved in the surrogate palette, the pre-exponential factors of the 10 most important reactions were optimised to better reproduce the oxidation rate of the single chemical species itself, similarly to what was done in the work of Cho et al. [53]. The chemistry tool of Convergent Science [55] was employed for such kind of activity, where a non-linear optimisation process was selected to reproduce the ignition delay times of the detailed chemical

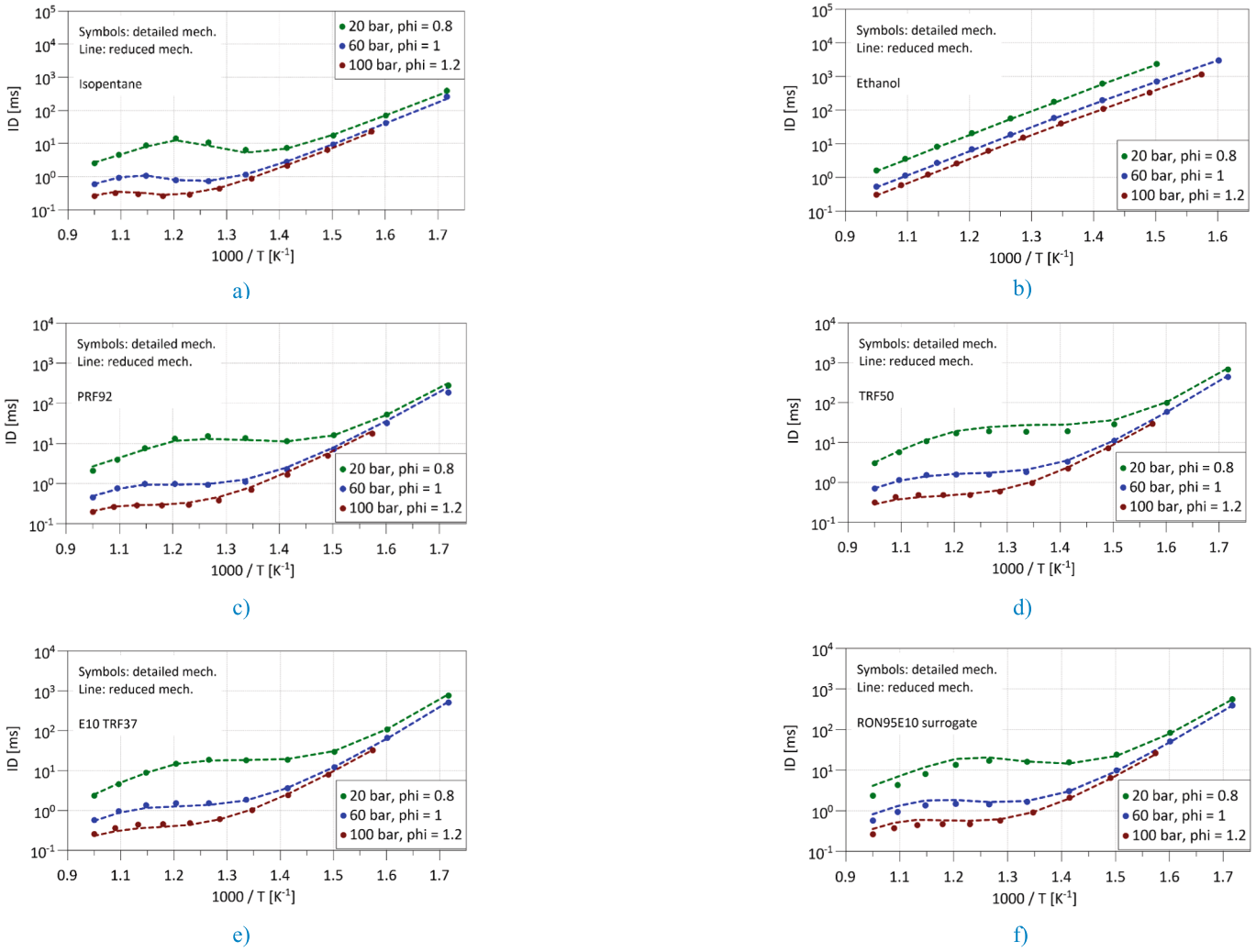

Fig. 9. Pure component and multicomponent mixtures ID_s comparison between detailed and reduced mechanisms: (a) Isopentane, (b) Ethanol, (c) PRF92, (d) TRF50, (e) E10 TRF37, (f) RON95E10 surrogate.

reaction mechanism at a pressure of 60 bar and 10 temperature levels starting from 600 K to 1000 K at stochiometric conditions. Fig. 7 sums up the overall adjustment of the pre-exponential factors of the final mechanism reactions with respect to DRGEPSA output one. It is to be specified that during the optimisation, the algorithm targeted the 10 reactions, also one at a time; therefore, the final number of optimised reactions could be lower than the number of surrogate chemical species multiplied by 10.

As can be seen from Fig. 7, the most important reactions which have been optimised (39 in total) are related to the initial dehydrogenation reactions of fuel surrogate species (IC_8, $C_6H_5CH_3$, IC_5H_{12}, NC_7H_{16}) by hydroxy (OH) or hydroperoxyl radical (HO_2) responsible of the NTC temperature region [53], as also pointed out by the sensitivity analysis carried out by Zhang et al. [26]. The major modifications are related to the aromatic species as well as the alkanes and isoalkanes hydrocarbon class (isooctane and n-heptane). In Fig. 8a–c, an example of the optimised ignition delay profile for isooctane, n-heptane and pseudocumene is reported. Particularly, the isooctane was affected by a lower reactivity with respect to the detailed mechanism, as the ignition delay was considerably higher than the reference one. This behaviour could be due to missing intermediate species removed by the DRGEPSA reduction process, which have altered the overall reactivity of the isooctane. By tuning the pre-exponential factor, the overall reactivity was corrected.

Fig. 9a and b highlight the performance of the reduced mechanism with respect to the comprehensive one for the single chemical species.

Table 9
PRF, TRF and ETRF mixture compositions used for reduced mechanism validation [53].

Chemical species	PRF92 [mol. %]	TRF50 [mol. %]	E10 TRF37 [mol. %]
Iso-octane	91.1 %	22.3 %	23.9 %
N-heptane	8.9 %	17.4 %	15.1 %
Toluene	0.0 %	60.3 %	41.0 %
Ethanol	0.0 %	0.0 %	20.0 %

Several thermodynamic conditions were tested, ranging from 20 to 100 bar for the pressure, 600 to 1000 K for the temperature, while the equivalence ratio was varied from 0.8 to 1.2, despite the reduction being carried out just in stochiometric conditions. As shown, the reduced mechanism can reproduce ID times of the detailed one with great accuracy at several temperatures, pressures and equivalence ratios. In the case of isopentane, the NTC ID region, between 700 and 900 K, is correctly captured by the reduced mechanism, proving that the overall species oxidation rate is maintained in the reduced mechanism. Moreover, to validate the reduced mechanism for mixtures, multicomponent fuels were tested, whose compositions are reported in Table 9. In particular, Primary Reference Fuel (PRF), Toluene Reference Fuel with and without ethanol (ETRF and TRF) and RON95E10 surrogate fuel generated in this work, were utilised for constant volume ID simulations with both the comprehensive and reduced mechanisms.

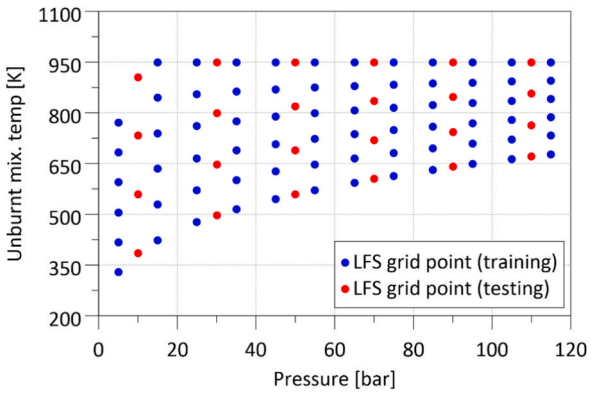

Fig. 10. Unburnt mixture temperature and in-cylinder pressure grid points for LFS simulations.

Table 10
LFS neural network training conditions.

	Pressure [bar]	Unburnt mix. T [K]	Equivalence ratio [–]	EGR [%]
Min	5	328	0.8	0
Max	115	950	1.2	30
Delta	10	6 steps for each pressure value	0.2	10

Table 11
LFS neural network testing conditions.

	Pressure [bar]	Unburnt mix. T [K]	Equivalence ratio [–]	EGR [%]
Min	10	328	0.9	5
Max	110	950	1.1	25
Delta	20	4 steps for each pressure value	0.2	10

Fig. 9c–f show some examples of the mixture ID times. For all four fuels, the high temperature and low temperature chemistry, as well as the NTC regions, are reproduced by the reduced mechanism, with slightly higher deviations for the RON95E10 surrogate at high temperature conditions.

3.4. Laminar flame speed chemical kinetics simulations

By following the approach of Del Pecchia et al. [67], the thermodynamic conditions to be used to perform chemical kinetics simulation for the LFS estimation were defined following a polytropic law, linking the unburnt mixture temperature, T_u, to the in-cylinder pressure, p_{cyl}. As shown in Fig. 10, both for RON95E10 and MtG – E10, high-pressure and low-temperature grid points were not simulated, since it is unlikely that an engine will operate in such conditions.

The LFS were estimated by employing the surrogate fuel formulations of Table 7 and the reduced chemical reaction mechanism. The overall thermodynamic conditions employed for LFS simulations are reported in Tables 10 and 11, both for training and testing the LFS neural networks for the 2 addressed fuels. For each couple of pressure and unburnt mixture temperature, a sweep in terms of EGR and equivalence ratio is performed. Overall, the training dataset consists of 864 points, whereby the neural networks are trained, while 144 are used for testing them, to assess their capability of predicting LFS not used for the training phase. It is worth highlighting the fact that the comprehensive mechanism was reduced for stochiometric conditions only, which can lead to some inaccuracies, as for laminar flame speed chemical kinetics simulation, for instance, in lean conditions. Lean LFS were nevertheless

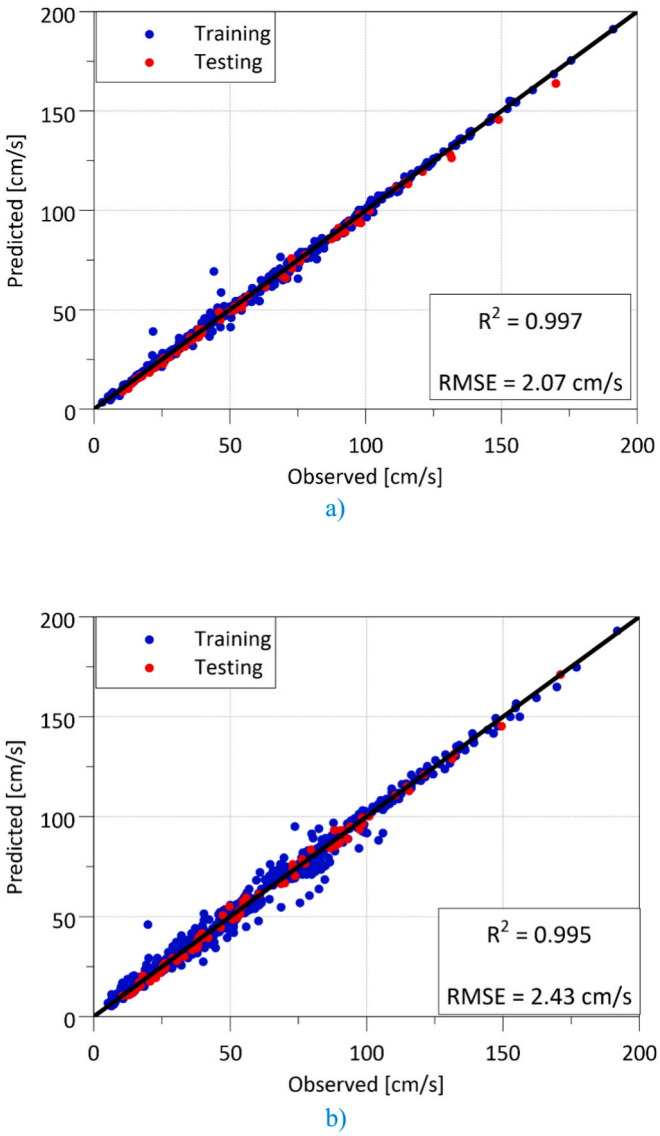

Fig. 11. Surrogate fuels laminar flame speed neural networks: (a) RON95E10, (b) MtG-E10.

simulated to provide the combustion model with reasonable values of LFS during simulation runtime, as, before reaching steady-state conditions, non-stoichiometric operation may arise. Training the LFS neural network just in stoichiometric conditions could lead to totally unphysical LFS predictions outside the training range. The chemistry tool embedded in the Converge software was used to solve the chemical kinetics simulations [55]. The software uses a premixed laminar flame speed model at constant pressure with a freely propagating flame in a one-dimensional channel with fixed cross-sectional area. The solver employed to solve the chemical kinetics simulation is Newton's solver, while the transport properties are calculated with a mixture-average approach from the input transport property file. The domain length was set to 0.1 m, with grid control parameters to achieve a cell number of around 260, representing a good compromise between accuracy and computational effort.

In this study, the LFS dataset was integrated into the predictive Eddy Burn Up combustion model, defined in the "EngCylCombSITurb" template, through the use of neural networks. Once the laminar flame speed values were simulated through chemical kinetics simulations, the GT-Post metamodel generator tool was employed and fed with the computed LFS. The input features to train the network are the same as

the ones used for the chemical kinetics simulations, and the output response is the LFS at that particular engine thermodynamic condition. For each surrogate fuel, a sweep of the most important hyperparameters was performed, such as the number of hidden layers, the number of neurons and the kind of hidden layer activation functions, to choose the best neural network for predicting the testing LFS dataset. For the training, a cross-validation logic was employed using 20 % of the training dataset for the network weights optimisation, preventing the networks from being overfit with such a validation method. The final RON95E10 LFS neural network consists of 2 hidden layers with 6 neurons each; the hidden layers' activation functions are hyperbolic tangent ones, while the output layer activation function is a linear one. Instead, for the MtG-E10 surrogate, the LFS neural network comprises only one hidden layer with 5 neurons, including a sigmoid activation function, while the output layer activation function is still a linear one. The difference in the complexity of the neural networks arises from the different LFS training datasets provided, especially regarding the LFS at EGR conditions, which led to a different combination of the optimal network's hyperparameters.

Fig. 11 depicts the performance of the neural networks featuring the highest coefficient of determination (R^2) and the lowest RMSE concerning the testing dataset. Both neural networks are able to replicate the testing dataset with good accuracy, as the coefficient of determination exceeds 0.95, and the RMSE for the testing dataset is really low. The GT-Post tool allows the user to export the metamodels to be integrated into the "EngCylCombSITurb" template as a custom LFS model. The next section highlights the results related to the Eddy-Burn Up combustion model calibration and testing for RON95E10, and its prediction assessment with MtG – E10 surrogate fuel.

3.5. Combustion model calibration and validation

As mentioned in Section 2, 18 engine operating points for standard RON95E10 fuel were employed to calibrate the Eddy-Burn Up combustion model (additional details about its mathematical formulation can be found in the work of Keck et al. [42] and Morel et al. [43]). The remaining 5 were used to test the model after its calibration, to verify the prediction behaviour of other engine operating points not used for calibration purposes. In addition, MtG – E10 combustion was assessed with the same model, and just the laminar flame speed neural network was changed according to the tested fuel. The combustion model calibration parameters were not varied while switching fuel kinds.

To calibrate the combustion model, all the experimental data coming from the engine test bench, both for RON95E10 and MtG – E10 fuels, were post-processed to come up with the mean engine cycle, in terms of mean intake/exhaust manifold pressure dynamics as well as the mean in-cylinder pressure profile. These quantities were fed into the 1D CFD model as inputs to perform the three-pressure analysis. This kind of simulation takes boundary data like the in-cylinder pressure, the intake and exhaust port pressures, the valve lifts/timings, the valve tumble coefficients, the spark timing, the boundary intake and exhaust temperatures and the intake EGR fraction, to estimate the in-cylinder conditions at intake valve closing (IVC). Other outputs of the TPA are the fuel burn rate and the simulated in-cylinder pressure when the estimated burn rate is imposed in the model. The estimated burn rates will serve as the reference for calibrating and testing the combustion model.

Once the reference burn rate profiles were obtained by three pressure analysis, the Eddy-Burn Up combustion model could be eventually calibrated. The latter takes as input two other key features, namely the turbulent kinetic energy (TKE) and integral length scale (L_i) profiles. These quantities describe the evolution of the turbulence level inside the cylinder, which is a crucial feature to be reproduced if a predictive combustion model is put into place. This flow model was previously calibrated by taking as reference TKE and L_i profiles, the ones resulting from a 3D CFD cold flow simulation at 2000 1/min and 15 bar IMEP. For the sake of brevity and since it is not the main topic of this work, the calibration procedure is omitted.

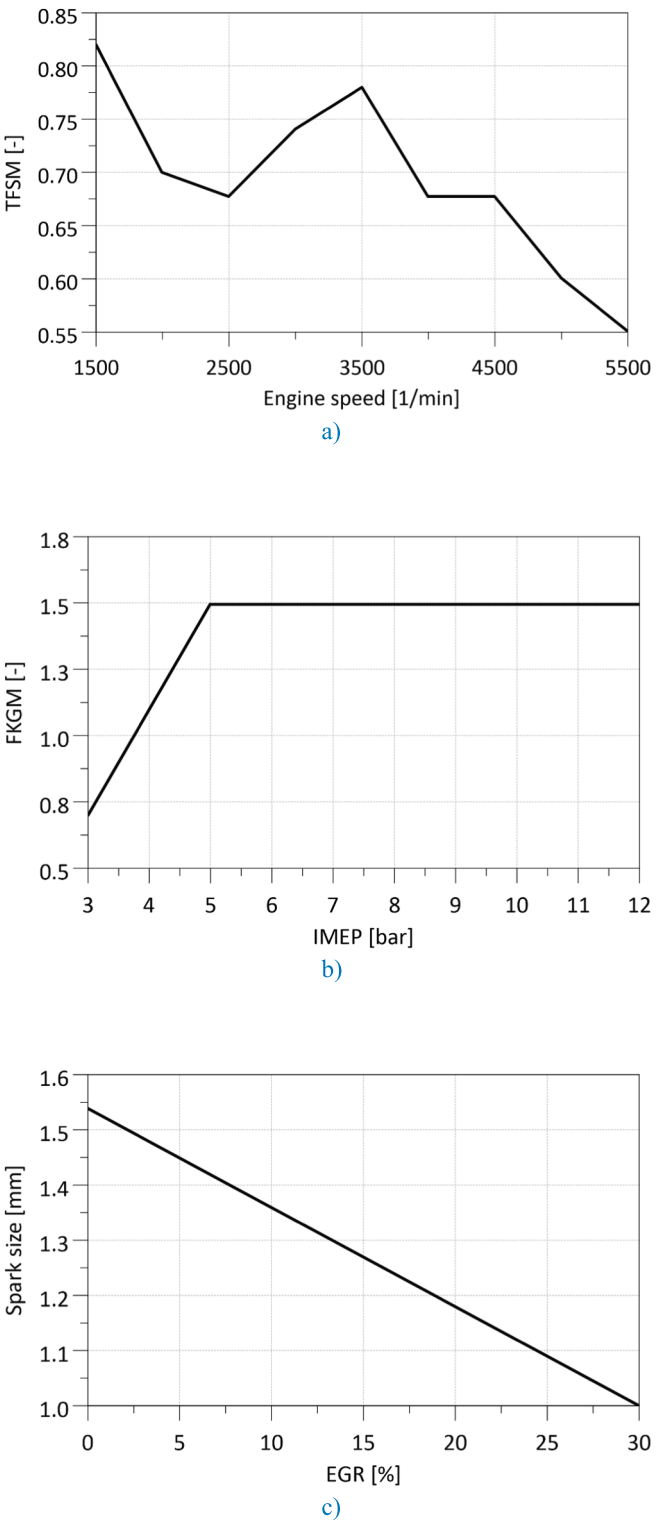

Fig. 12. Turbulent flame speed parameter maps: (a) turbulent flame speed multiplier, (b) flame kernel growth multiplier, (c) initial spark size.

The combustion model parameters were calibrated through a closed volume analysis, that is, the TPA model was simplified as just the cylinder, the injector and the engine templates were kept in the model. The IVC initial conditions were estimated by the three-pressure analysis and loaded into the simplified model. The GT-Suite Integrated Design Optimiser was employed to estimate the parameters that minimised the

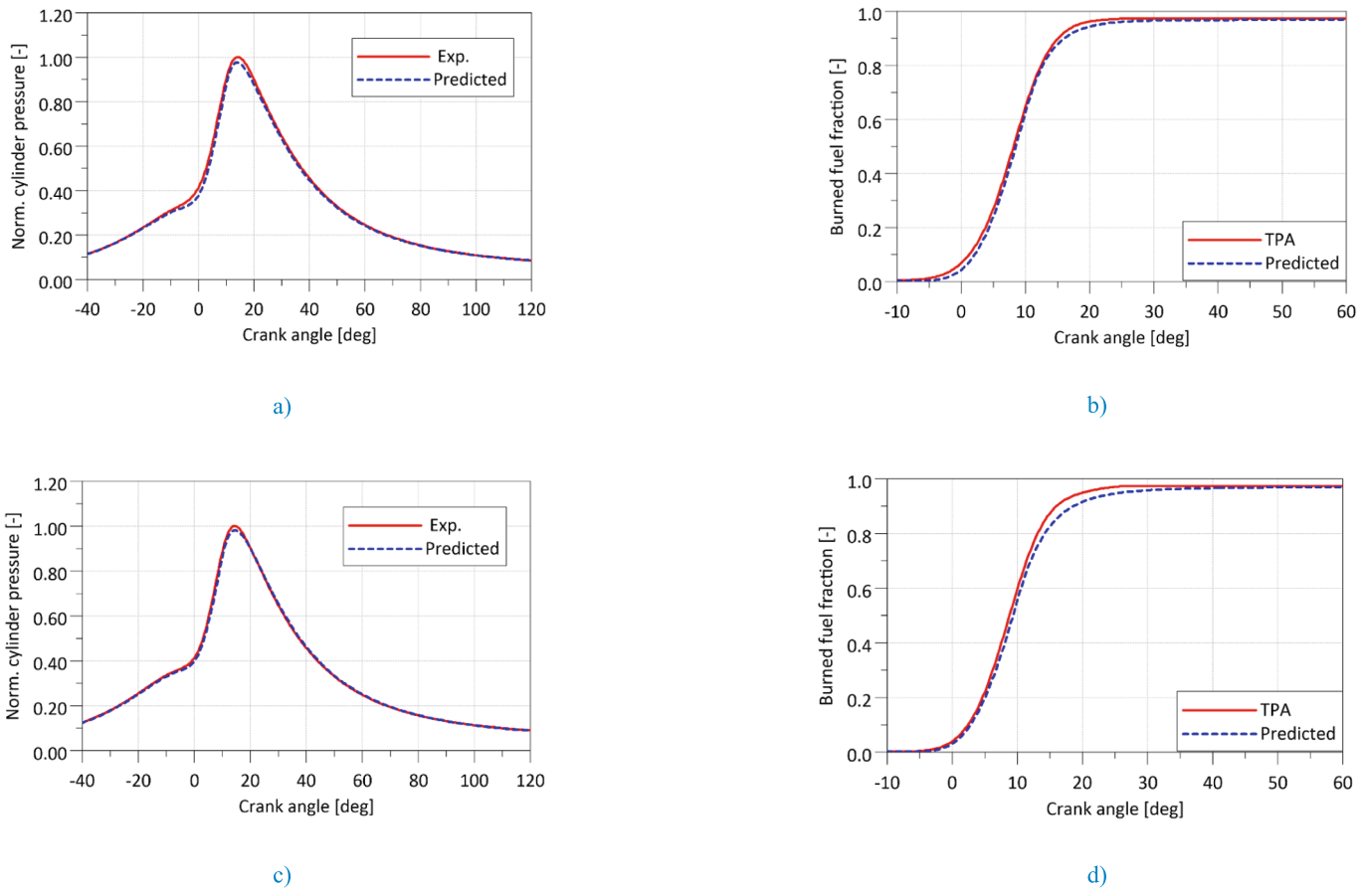

Fig. 13. Combustion model calibration and validation for RON95E10. (a) Calibration dataset: 2000 RPM, 12 bar IMEP, 10 % EGR in-cylinder pressure, (b) calibration dataset: 2000 RPM, 12 bar IMEP, 10 % EGR burned fuel fraction, (c) testing dataset: 3000 RPM, 6 bar IMEP in cylinder pressure, (d) testing dataset: 3000 RPM, 6 bar IMEP burned fuel fraction.

"Improved Burn Rate RMS Error (Meas vs Pred)" among the 18 cases for RON95E10 gasoline fuel. The resulting tuned parameters were further manually adjusted, since a single constant set was not enough to reproduce properly all the engine operating points. Specifically, by following the work of Guarnieri [68], the turbulent flame speed multiplier was adjusted according to the engine speed (Fig. 12a). This tuning could be related to the level of turbulence inside the cylinder, which is not properly captured by the 0D turbulence model, as its calibration was

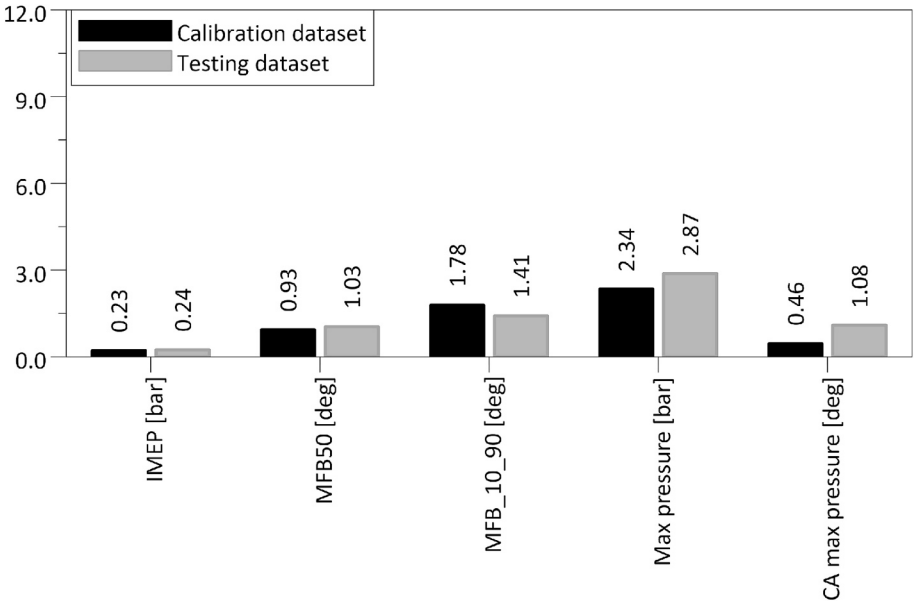

Fig. 14. RMSE of key combustion metrics for the RON95E10 predictive combustion model compared to the TPA reference values.

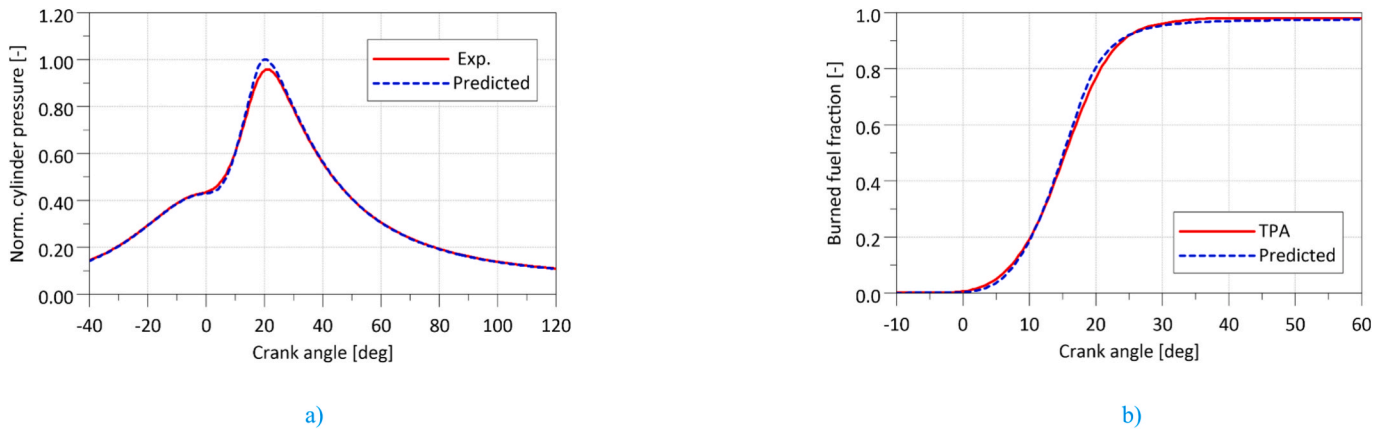

Fig. 15. Combustion model testing for MtG-E10 at 2500 RPM, 16 bar IMEP, 10 % EGR: (a) in-cylinder pressure, (b) burned fuel fraction.

performed on only one available engine operating point (2000 1/min and 15 bar IMEP), for which reference 3D CFD turbulent kinetic energy and integral length scale profiles were available. Moreover, as pointed out also by Sok et al. [69], the turbulence intensity, u', is also influenced by the prediction of the in-cylinder mass and, in their work, the Turbulent Flame Speed Multiplier (TFSM) was adjusted as well. The Flame Kernel Growth Multiplier (FKGM) was reduced to improve the predictions at low load conditions (Fig. 12b). This was needed to better predict the maximum pressure and the crank angle at the maximum pressure, as the parameter from the output of the optimisation was leading to an overprediction of the in-cylinder pressure. The reason for such deviation is possibly related to the prediction of the right turbulence level at low load conditions, in which the role of the injection phase has a higher impact on the overall turbulence level [70,71]. Above 5 bar IMEP, this parameter is constant and equal to the output of the optimisation procedure. As for the Taylor Length Scale Multiplier, it was kept fixed at 2.989. Moreover, the spark size was adjusted according to the EGR concentration (Fig. 12c), since, as pointed out by Zhen et al. [72], the ignition delay time increases with the EGR% most likely due to the smaller initial flame kernel radius. A linear correlation was employed in this study to deal with this kind of effect, since the combustion model does not include a phenomenological representation of the formation of the initial kernel size. The spark size at 0 % of EGR was coming out of the optimisation process of the combustion parameters, while the one at 30 % was manually adjusted to reproduce the heat release at the maximum EGR rate. The linear correlation was then utilised to deal with intermediate EGR rate percentages.

Fig. 13 shows some examples of the performance of the combustion model with respect to the experimental counterpart, both for the calibration and testing engine OPs. Additional ones are provided in the Supplementary Material. As can be seen, the combustion model, once calibrated, is able to replicate the reference burn fuel fraction profiles and the in-cylinder pressure at several engine speeds and loads. Moreover, the most crucial combustion metrics quantities were evaluated in terms of RMSE against the reference counterpart, as shown in Fig. 14. The overall combustion phasing is well reproduced, as the MFB50 and MFB1090 RMSEs are below 1° and 2°, respectively. A slightly higher error can be seen for the maximum pressure, even if below 3 bars.

Eventually, to verify the ability of the model to keep its predictive capability while switching fuel kinds, MtG – E10 fuel was addressed. The RON95E10 LFS metamodel was replaced with the MtG – E10 one, and the turbulent flame speed parameters were not recalibrated in this regard. It is widely acknowledged that the combustion in an ICE occurs in the so-called “wrinkled or corrugated flamelet” regimes [73], in which the flame front thickness is smaller than the lowest turbulent length scale (Kolmogorov scale). This implies that the turbulence does not

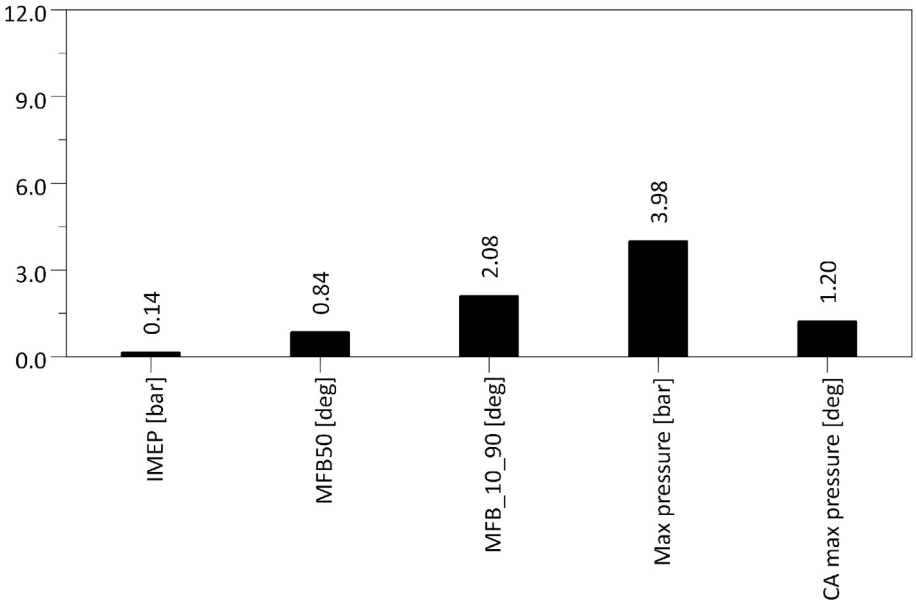

Fig. 16. RMSE of key combustion metrics for the MtG-E10 predictive combustion model compared to the TPA reference values.

change the inner flame structure, and the laminar flame speed synthesises the chemical kinetics occurring within the flame front. Again, a closed volume analysis was performed by starting the simulations with the TPA IVC in-cylinder initial conditions. As depicted in Fig. 15, the combustion model is able to predict the burned fuel fraction profiles with great accuracy, as also shown by the additional plots reported in the Supplementary Material. Fig. 16 summarises the overall prediction performance. As reported in the bar plot, the combustion phasing is well reproduced, as well as the maximum pressure, which is affected by a slight overestimation. These findings align with a recent similar study by Esposito et al. [74], even if not entirely focused on gasoline-like fuels, in which the 0D combustion model was calibrated for neat methanol fuel and then tested for three gasoline engine operating points at the same speed but different loads. There, the MFB50 was imposed as the combustion anchoring angle, while the SA was adjusted by the solver. This study, instead, set the same test bench SA and the MFB50 is a consequence of the combustion model, enabling the possibility of building control strategies based on the SA angle rather than the MFB50. The main limitation of the model testing is that the experimental engine OP_s for MtG-E10 fuel were only available at a single engine speed, 2500 1/min. Nevertheless, this synthetic fuel is meant to mimic the overall characteristics of the fossil fuel counterpart, RON95E10. Therefore, the combustion behaviour for the MtG-E10 fuel is expected to be quite similar to the fossil one.

4. Conclusions

This study provides a methodology for combustion simulation of RON95E10 and MtG-E10 fuels. They were tested in a single-cylinder spark-ignited research engine, and a surrogate fuel algorithm was developed to determine equivalent fuel composition replicating target characteristics like density, RON/MON, CHR, VO%, and evaporation properties. A physical model for the distillation process was developed and validated against literature data. The surrogate species palette included hydrocarbons from C5 to C9 to cover the gasoline distillation spectrum, and an optimisation algorithm determined the best surrogate fuel composition. For LFS chemical kinetics simulations, the LLNL mechanism [40] with NO_x chemistry [61] was reduced via DRGEPSA. The reduced mechanism, featuring 548 species and 3350 reactions, was validated for ID times with mixtures from PRF to RON95E10 surrogate composition. LFS neural networks were built using simulated data at representative engine conditions. The Eddy-Burn Up model was calibrated with 18 RON95E10 engine operating points and tested with 5, showing good accuracy. The MFB50 and MFB1090 RMSEs are below 1° and 2°, respectively, while the one for the maximum pressure is below 3 bars. The model's predictive capability was tested with MtG-E10 by just replacing the LFS neural network in the combustion model. Results showed in-cylinder pressure RMSE below 4 bars and MFB50 error less than 1°. The methodology paves the way for defining surrogate mixtures of synthetic gasoline fuels for combustion simulation and evaporation analysis. Future work could investigate some limitations of the present one, such as including cycloalkanes in the surrogate palette to come up with a complete surrogate composition representative of all the hydrocarbon classes. In addition, the analysis could be extended to predict the main engine out emissions, such as NOx, HC and CO, coupled with the predictions of the calibrated combustion model.

Funding sources

This research did not receive any specific grant from funding agencies in the public, commercial, or not-for-profit sectors.

CRediT authorship contribution statement

Lorenzo Ferrari: Writing – review & editing, Writing – original draft, Visualization, Validation, Methodology, Investigation. **Massimo Duchi:** Writing – review & editing, Validation, Methodology, Investigation. **Giuseppe Sammito:** Validation, Supervision, Project administration. **Marcus Fischer:** Validation, Supervision, Project administration, Data curation. **Nicolò Cavina:** Validation, Supervision, Software, Project administration.

Declaration of competing interest

The authors declare that they have no known competing financial interests or personal relationships that could have appeared to influence the work reported in this paper.

Acknowledgments

The authors are thankful to Convergent Science for providing CONVERGE licenses.

Appendix A. Supplementary data

Supplementary data to this article can be found online at https://doi.org/10.1016/j.enconman.2025.120968.

Data availability

The data that has been used is confidential.

References

[1] 'Secretary-General's remarks at closing of Climate Action Summit [as delivered] | United Nations Secretary-General'. Accessed: Apr. 28, 2025. [Online]. Available: https://www.un.org/sg/en/content/sg/statement/2019-09-23/secretary-generals-remarks-closing-of-climate-action-summit-delivered.
[2] K. Calvin et al., 'IPCC, 2023: Climate Change 2023: Synthesis Report. Contribution of Working Groups I, II and III to the Sixth Assessment Report of the Intergovernmental Panel on Climate Change [Core Writing Team, H. Lee and J. Romero (eds.)]. IPCC, Geneva, Switzerland.', Intergovernmental Panel on Climate Change (IPCC), Jul. 2023. doi: 10.59327/IPCC/AR6-9789291691647.
[3] 'Delivering the European Green Deal - European Commission'. Accessed: Mar. 05, 2025. [Online]. Available: https://commission.europa.eu/strategy-and-policy/priorities-2019-2024/european-green-deal/delivering-european-green-deal_en.
[4] 'IEA (2023), Road transport, IEA, Paris https://www.iea.org/reports/road-transport, Licence: CC BY 4.0', IEA.
[5] Peng B-B, Fan Y, Xu J-H. Integrated assessment of energy efficiency technologies and CO2 abatement cost curves in China's road passenger car sector. Energy Convers Manag Feb. 2016;109:195–212. https://doi.org/10.1016/j.enconman.2015.11.064.
[6] J. A. García Sánchez, J. M. López Martínez, J. Lumbreras Martín, M. N. Flores Holgado, and H. Aguilar Morales, 'Impact of Spanish electricity mix, over the period 2008–2030, on the Life Cycle energy consumption and GHG emissions of Electric, Hybrid Diesel-Electric, Fuel Cell Hybrid and Diesel Bus of the Madrid Transportation System', Energy Convers. Manag., vol. 74, pp. 332–343, Oct. 2013, doi: 10.1016/j.enconman.2013.05.023.
[7] Lester MS, Bramstoft R, Münster M. Analysis on Electrofuels in Future Energy Systems: a 2050 Case Study. Energy May 2020;199:117408. https://doi.org/10.1016/j.energy.2020.117408.
[8] 'Schmidt PR, Zittel W, Weindorf W, Raksha T. Renewables in transport 2050, tech. Rep.. Frankfurt: Research Association for Combustion Engines; 2016. www.fvv-net.de'.
[9] Grahn M, Azar C, Lindgren K. The role of biofuels for transportation in CO2 emission reduction scenarios with global versus regional carbon caps. Biomass Bioenergy 2009;33(3):360–71. https://doi.org/10.1016/j.biombioe.2008.08.019.
[10] Nemmour A, Inayat A, Janajreh I, Ghenai C. Green hydrogen-based E-fuels (E-methane, E-methanol, E-ammonia) to support clean energy transition: a literature review. Int J Hydrog Energy 2023;48(75):29011–33. https://doi.org/10.1016/j.ijhydene.2023.03.240.
[11] Dieterich V, Buttler A, Hanel A, Spliethoff H, Fendt S. Power-to-liquid via synthesis of methanol, DME or Fischer–Tropsch-fuels: a review. Energy Environ Sci 2020;13(10):3207–52. https://doi.org/10.1039/D0EE01187H.
[12] Dell'Aversano S, Villante C, Gallucci K, Vanga G, Di Giuliano A. E-fuels: a comprehensive review of the most promising technological alternatives towards an energy transition. Energies 2024;17(16):3995. https://doi.org/10.3390/en17163995.
[13] Ababneh H, Hameed BH. Electrofuels as emerging new green alternative fuel: a review of recent literature. Energy Convers Manag 2022;254:115213. https://doi.org/10.1016/j.enconman.2022.115213.

[14] Wouters C, et al. Evaluation of synthetic gasoline fuels and alcohol blends in a spark-ignition engine, SAE Int J Fuels Lubr 2022; 15(3): 04-15-03–0017. doi: 10.4271/04-15-03-0017.
[15] Yarulina I, Chowdhury AD, Meirer F, Weckhuysen BM, Gascon J. Recent trends and fundamental insights in the methanol-to-hydrocarbons process. Nat Catal 2018;1 (6):398–411. https://doi.org/10.1038/s41929-018-0078-5.
[16] Kraus C, Fitz P, Fellner F, Härtl M, Jaensch M. Exhaust gas analysis of various potential GHG-neutral synthetic fuels and gasoline/alkylate-blends including variable injection timings. In: Presented at the SAE Powertrains Fuels & Lubricants Conference & Exhibition; 2022. https://doi.org/10.4271/2022-01-1085. pp. 2022–01–1085.
[17] J. Villforth, A. C. Kulzer, A. Weißhaar, H.-P. Deeg, and M. Bargende, 'The Influence of eFuel Formulation on Post Oxidation and Cold Start Emissions', presented at the SAE WCX Digital Summit, Apr. 2021, pp. 2021-01–0632. doi: 10.4271/2021-01-0632.
[18] Albrecht M, Deeg H-P, Schwarzenthal D, Eilts P. The influence of fuel composition and renewable fuel components on the emissions of a GDI engine. Presented at the CO2 reduction for transportation systems conference; 2020. p. 2020-37–0025. doi: 10.4271/2020-37-0025.
[19] Rossi E, et al. Experimental and numerical investigation for improved mixture formation of an eFuel compared to standard gasoline. pp. 2021–24–0019. In: Presented at the 15th International Conference on Engines & Vehicles; 2021. https://doi.org/10.4271/2021-24-0019.
[20] Pitz WJ et al. Development of an experimental database and chemical kinetic models for surrogate gasoline fuels, Presented at the SAE world congress & exhibition; 2007. p. 2007-01–0175. doi: 10.4271/2007-01-0175.
[21] Grubinger T, Lenk G, Schubert N, Wallek T. Surrogate generation and evaluation of gasolines. Fuel 2021;283:118642. https://doi.org/10.1016/j.fuel.2020.118642.
[22] Vajda S, Valko P, Turányi T. Principal component analysis of kinetic models. Int J Chem Kinet 1985;17(1):55–81. https://doi.org/10.1002/kin.550170107.
[23] Turányi T. Sensitivity analysis of complex kinetic systems. Tools and applications. J Math Chem 1990;5(3):203–48. https://doi.org/10.1007/BF01166355.
[24] Turanyi T. Reduction of large reaction mechanisms. Reduct Large React Mech 1990;14(11):795–803.
[25] Wang H, Frenklach M. Detailed reduction of reaction mechanisms for flame modeling. Combust Flame 1991;87(3):365–70. https://doi.org/10.1016/0010-2180(91)90120-Z.
[26] Zhang L, Qi Q. A reduced mechanism for the combustion of gasoline-ethanol blend on advanced engine combustion modes. Fuel 2021;300:120951. https://doi.org/10.1016/j.fuel.2021.120951.
[27] He K, Androulakis IP, Ierapetritou MG. Multi-element flux analysis for the incorporation of detailed kinetic mechanisms in reactive simulations. Energy Fuels 2010;24(1):309–17. https://doi.org/10.1021/ef900803q.
[28] Lu T, Law CK. A directed relation graph method for mechanism reduction. Proc Combust Inst 2005;30(1):1333–41. https://doi.org/10.1016/j.proci.2004.08.145.
[29] Lu T, Law CK. Linear time reduction of large kinetic mechanisms with directed relation graph: n-Heptane and iso-octane. Combust Flame 2006;144(1):24–36. https://doi.org/10.1016/j.combustflame.2005.02.015.
[30] Luo Z, Lu T, Maciaszek MJ, Som S, Longman DE. A reduced mechanism for high-temperature oxidation of biodiesel surrogates. Energy Fuels 2010;24(12):6283–93. https://doi.org/10.1021/ef1012227.
[31] Pepiot-Desjardins P, Pitsch H. An efficient error-propagation-based reduction method for large chemical kinetic mechanisms. Combust Flame 2008;154(1): 67–81. https://doi.org/10.1016/j.combustflame.2007.10.020.
[32] Zheng XL, Lu TF, Law CK. Experimental counterflow ignition temperatures and reaction mechanisms of 1,3-butadiene. Proc Combust Inst 2007;31(1):367–75. https://doi.org/10.1016/j.proci.2006.07.182.
[33] Niemeyer KE, Sung C-J, Raju MP. Skeletal mechanism generation for surrogate fuels using directed relation graph with error propagation and sensitivity analysis. Combust Flame 2010;157(9):1760–70. https://doi.org/10.1016/j.combustflame.2009.12.022.
[34] Sarathy SM, Farooq A, Kalghatgi GT. Recent progress in gasoline surrogate fuels. Prog Energy Combust Sci 2018;65:67–108. https://doi.org/10.1016/j.pecs.2017.09.004.
[35] Chen Y, Wolk B, Mehl M, Cheng WK, Chen J-Y, Dibble RW. Development of a reduced chemical mechanism targeted for a 5-component gasoline surrogate: a case study on the heat release nature in a GCI engine. Combust Flame 2017;178: 268–76. https://doi.org/10.1016/j.combustflame.2016.12.018.
[36] Mehl M, Pitz WJ, Westbrook CK, Curran HJ. Kinetic modeling of gasoline surrogate components and mixtures under engine conditions. Proc Combust Inst 2011;33(1): 193–200. https://doi.org/10.1016/j.proci.2010.05.027.
[37] Andrae JCG, Head RA. HCCI experiments with gasoline surrogate fuels modeled by a semidetailed chemical kinetic model. Combust Flame 2009;156(4):842–51. https://doi.org/10.1016/j.combustflame.2008.10.002.
[38] Zhong B-J, Zheng D. A chemical mechanism for ignition and oxidation of multi-component gasoline surrogate fuels. Fuel 2014;128:458–66. https://doi.org/10.1016/j.fuel.2014.03.044.
[39] Kukkadapu G, Kumar K, Sung C-J, Mehl M, Pitz WJ. Experimental and surrogate modeling study of gasoline ignition in a rapid compression machine. Combust Flame 2012;159(10):3066–78. https://doi.org/10.1016/j.combustflame.2012.05.008.
[40] Cheng S, et al. Autoignition and preliminary heat release of gasoline surrogates and their blends with ethanol at engine-relevant conditions: experiments and comprehensive kinetic modeling. Combust Flame 2021;228:57–77. https://doi.org/10.1016/j.combustflame.2021.01.033.
[41] 'Welcome to Gamma Technologies - home of GT-SUITE system simulation software', Gamma Technologies. Accessed: Mar. 12, 2025. [Online]. Available: https://www.gtisoft.com/.
[42] Keck JC, Heywood JB, Noske G, Keck JC, Heywood JB, Noske G. Early flame development and burning rates in spark ignition engines and their cyclic variability. In: Presented at the SAE International Congress and Exposition. SAE International; 1987. https://doi.org/10.4271/870164.
[43] Morel T, et al. Model for heat transfer and combustion in spark ignited engines and its comparison with experiments. In: Presented at the SAE International Congress and Exposition. SAE International; 1988. https://doi.org/10.4271/880198.
[44] Ahmed A, Goteng G, Shankar VSB, Al-Qurashi K, Roberts WL, Sarathy SM. A computational methodology for formulating gasoline surrogate fuels with accurate physical and chemical kinetic properties. Fuel 2015;143:290–300. https://doi.org/10.1016/j.fuel.2014.11.022.
[45] Kim D, Song J, Song H, Lim Y, Lee S, Song HH. Assessment of hydrocarbons for gasoline surrogate: an optimization study. Fuel 2022;328:125286. https://doi.org/10.1016/j.fuel.2022.125286.
[46] Bozza F, De Bellis V, Dulbecco A. Advanced 0D and QuasiD thermodynamic combustion models for SI and CI engines, USA; 2020. [Online]. Available: https://www.iris.unina.it/handle/11588/952729.2 [accessed: Mar. 07, 2025].
[47] Sarathy SM, et al. Compositional effects on the ignition of FACE gasolines. Combust Flame 2016;169:171–93. https://doi.org/10.1016/j.combustflame.2016.04.010.
[48] Daly SR, Niemeyer KE, Cannella WJ, Hagen CL. FACE gasoline surrogates formulated by an enhanced multivariate optimization framework. Energy Fuels 2018;32(7):7916–32. https://doi.org/10.1021/acs.energyfuels.8b01313.
[49] Anderson JE, et al. Octane numbers of ethanol-gasoline blends: measurements and novel estimation method from molar composition. Presented at the SAE 2012 world congress & exhibition; 2012. p. 2012-01–1274. doi: 10.4271/2012-01-1274.
[50] Mariani V, Pulga L, Bianchi GM, Falfari S, Forte C. Machine learning-based identification strategy of fuel surrogates for the CFD simulation of stratified operations in low temperature combustion modes. Energies 2021;14(15):4623. https://doi.org/10.3390/en14154623.
[51] EN ISO 3405:2011 Petroleum products —Determination of distillation characteristics at atmospheric pressure; 2011.
[52] Ahmed T. Chapter 5 - equations of state and phase equilibria. In: Ahmed T, editor. Equations of state and PVT analysis, 2nd ed., Boston: Gulf Professional Publishing; 2016. p. 467–597. doi: 10.1016/B978-0-12-801570-4.00005-2.
[53] Cho S, Lopez-Pintor D, Sofianopoulos A. A skeletal mechanism for gasoline surrogates: development, validation, and CFD application. Fuel 2023;332:126236. https://doi.org/10.1016/j.fuel.2022.126236.
[54] Chen Y, Mehl M, Xie Y, Chen J-Y. Improved skeletal reduction on multiple gasoline-ethanol surrogates using a Jacobian-aided DRGEP approach under gasoline compression ignition (GCI) engine conditions. Fuel 2017;210:617–24. https://doi.org/10.1016/j.fuel.2017.08.085.
[55] 'Richards KJ, Senecal PK, Pomraning E. CONVERGE 4.1, Convergent Science, Madison, WI; 2025.
[56] Bruno TJ, Smith BL. Evaluation of the physicochemical authenticity of aviation kerosene surrogate mixtures. Part 1: Analysis of volatility with the advanced distillation curve. Energy Fuels 2010;24(8):4266–76. https://doi.org/10.1021/ef100496j.
[57] Gail S, et al. Evaluating a novel gasoline surrogate containing isopentane using a rapid compression machine and an engine. Proc Combust Inst 2021;38(4): 5643–53. https://doi.org/10.1016/j.proci.2020.07.103.
[58] Hutchison BRM, Wallace JS. Influence of fuel volatility on particulate matter emissions from a production DISI engine. Fuel 2021;303:121206. https://doi.org/10.1016/j.fuel.2021.121206.
[59] Zhu R, Hu J, Bao X, He L, Zu L. Effects of aromatics, olefins and distillation temperatures (T50 & T90) on particle mass and number emissions from gasoline direct injection (GDI) vehicles. Energy Policy Feb. 2017;101:185–93. https://doi.org/10.1016/j.enpol.2016.11.022.
[60] Badra J, AlRamadan AS, Sarathy SM. Optimization of the octane response of gasoline/ethanol blends. Appl Energy 2017;203:778–93. https://doi.org/10.1016/j.apenergy.2017.06.084.
[61] 'Chemical-Kinetic Mechanisms for Combustion Applications, San Diego Mechanism web page, Mechanical and Aerospace Engineering (Combustion Research), University of California at San Diego (http://combustion.ucsd.edu)'.
[62] Brezinsky K. The high-temperature oxidation of aromatic hydrocarbons. Prog Energy Combust Sci 1986;12(1):1–24. https://doi.org/10.1016/0360-1285(86)90011-0.
[63] Simmie JM. Detailed chemical kinetic models for the combustion of hydrocarbon fuels. Prog Energy Combust Sci 2003;29(6):599–634. https://doi.org/10.1016/S0360-1285(03)00060-1.
[64] Jin H, et al. Combustion chemistry of aromatic hydrocarbons. Prog Energy Combust Sci 2023;96:101076. https://doi.org/10.1016/j.pecs.2023.101076.
[65] Cai L, Pitsch H. Optimized chemical mechanism for combustion of gasoline surrogate fuels. Combust Flame 2015;162(5):1623–37. https://doi.org/10.1016/j.combustflame.2014.11.018.
[66] Mehl M, Chen JY, Pitz WJ, Sarathy SM, Westbrook CK. An approach for formulating surrogates for gasoline with application toward a reduced surrogate mechanism for CFD engine modeling. Energy Fuels 2011;25(11):5215–23. https://doi.org/10.1021/ef201099y.
[67] Del Pecchia M, Pessina V, Berni F, d'Adamo A, Fontanesi S. Gasoline-ethanol blend formulation to mimic laminar flame speed and auto-ignition quality in automotive engines. Fuel 2020;264:116741. https://doi.org/10.1016/j.fuel.2019.116741.

[68] Guarnieri M. Calibration and assessment of the capability of the predictive combustion model SI-Turb. laurea, Politecnico di Torino, 2018. <https://webthesis.biblio.polito.it/8665/> [accessed: Aug. 11, 2024].
[69] Sok R, Yamaguchi K, Kusaka J. 0D/1D turbulent combustion model assessment from an ultra-lean spark ignition engine. Presented at the Asia-Pacific automotive engineering conference; Mar 2019. p. 2019-01–1409. doi: 10.4271/2019-01-1409.
[70] Song J, Kim T, Jang J, Park S. Effects of the injection strategy on the mixture formation and combustion characteristics in a DISI (direct injection spark ignition) optical engine. Energy 2015;93:1758–68. https://doi.org/10.1016/j.energy.2015.10.058.
[71] Kim D, Son Y, Park S. Effects of fuel injection on turbulence enhancement in a spray-guided, gasoline direct-injection, optically accessible engine with a high-pressure injection system. Presented at the WCX SAE World Congress Experience, Detroit, Michigan, United States, Apr. 2023, pp. 2023-01–0216. doi: 10.4271/2023-01-0216.
[72] Zhen X, Li X, Wang Y, Liu D, Tian Z, Wang Y. Effects of the initial flame kernel radius and EGR rate on the performance, combustion and emission of high-compression spark-ignition methanol engine. Fuel 2020;262:116633. https://doi.org/10.1016/j.fuel.2019.116633.
[73] Onorati A, Montenegro G. 1D and multi-D modeling techniques for IC engine simulation. SAE Int 2020. https://doi.org/10.4271/9780768099522.
[74] Esposito S, et al. Methanol fuelling of a spark-ignition engine: experiments and 0D/1D predictive modelling for combustion, performance, and emissions. Fuel 2025;393:134657. https://doi.org/10.1016/j.fuel.2025.134657.